AD_____

Award Number:
W81XWH-11-1-0442

TITLE:
Nanomedicine for early disease detection and treatment

PRINCIPAL INVESTIGATOR:
Ching-Hsuan Tung, PhD

CONTRACTING ORGANIZATION:
Methodist Hospital Research Institute
Houston, TX 77030

REPORT DATE:
September 2013

TYPE OF REPORT:
Final Report

PREPARED FOR: U.S. Army Medical Research and Materiel Command
Fort Detrick, Maryland 21702-5012

REPORT DOCUMENTATION PAGE

Form Approved
OMB No. 0704-0188

1. REPORT DATE	2. REPORT TYPE	3. DATES COVERED
September 2013	Final Report	15 August 2011—14 August 2013

4. TITLE AND SUBTITLE
NANOMEDICINE FOR EARLY DISEARS DETECTION AND TREATMENT

5a. CONTRACT NUMBER

5b. GRANT NUMBER
W81XWH-11-1-0442

5c. PROGRAM ELEMENT NUMBER

6. AUTHOR(S)
Ching-Hsuan Tung

E-Mail: ctung@HoustonMethodist.org

5d. PROJECT NUMBER

5e. TASK NUMBER

5f. WORK UNIT NUMBER

8. PERFORMING ORGANIZATION REPORT NUMBER

7. PERFORMING ORGANIZATION NAME(S) AND ADDRESS(ES)
Methodist Hospital Research Institute
Houston, TX 77030

9. SPONSORING / MONITORING AGENCY NAME(S) AND ADDRESS(ES)
U.S. Army Medical Research and Materiel Command

Fort Detrick, Maryland 21702-5012

10. SPONSOR/MONITOR'S ACRONYM(S)

11. SPONSOR/MONITOR'S REPORT NUMBER(S)

12. DISTRIBUTION / AVAILABILITY STATEMENT
Approved for Public Release; Distribution Unlimited

13. SUPPLEMENTARY NOTES

14. ABSTRACT
A platform technology to prepare enzyme sensitive nanomedicine (ESNM), which integrates the imaging and treatment capability, has been developed to report and cure diseases. ESNM is prepared with multiple layers of polyelectrolytes, sequentially assembled on an inert gold nanoparticle, using alternating charged polymers. Potentially the release kinetics could be controlled by varying polyelectrolytes with different properties, such as length, ionic strength and bond stability. Upon incubation with cells, the assembled ESNMs are taken up efficiently. The tight packing and layered assembly of the quenched polyelectrolytes slow subsequent intracellular degradation, and then result in a prolonged intracellular fluorescence signal and therapeutic effect for up to 3 weeks with no noticeable toxicity.

15. SUBJECT TERMS
Nanomedicine, imaging, siRNA, delivery, activation, enzyme, protease

16. SECURITY CLASSIFICATION OF:			17. LIMITATION OF ABSTRACT	18. NUMBER OF PAGES	19a. NAME OF RESPONSIBLE PERSON
a. REPORT	b. ABSTRACT	c. THIS PAGE			USAMRMC
U	U	U	UU	51	19b. TELEPHONE NUMBER *(include area code)*

Table of Contents

INTRODUCTION:

"Personalized medicine" is a goal for future medicine. However, many requirements need to be satisfied before "personalized medicine" can become a reality. In this new paradigm only those patients determined to have a high probability of responding to a particular therapeutic regimen will be given the selected treatment. This requires a diagnostic regime that can match the molecular characteristics of the patient and his/her specific diseased tissues with the treatment. In order to maximize therapeutic effects and minimize side effects the treatment should be targeted to modulate specific molecular pathways in specific tissues or cell types with high therapeutic index or target to background ratios. During the treatment phase, specific surrogate biomarkers will be needed to monitor the response of the diseased tissues to the treatment so that the treatment dose and regimen can be modified on a rational and ongoing basis. Since imaging can potentially be used to monitor molecular events *in vivo* in a spatially and temporally resolved manner non-invasively, a combined targeted imaging and therapy approach may be useful for achieving "personalized medicine". Advances in nanotechnology are expected to lead to the development of new and improved therapeutic strategies, amenable to targeting, that may ultimately revolutionize treatment. The specific aims of this study is to develop a platform technology for a novel type of multiplex enzyme sensitive nanomedicine (ESNM). The developed ESNM could be applied to image disease associated enzyme activity, and to have enzyme dependent therapeutic efficacy.

BODY:

Aim 1: Model system to demonstrate the enzyme activation strategy.

Severe invasive infections caused by highly virulent strains of group A Streptococcus (GAS) are serious medical problems in US. The GAS cysteine protease, SpeB (streptococcal pyrogenic exotoxin B), is one of the most important virulence factors produced by the organism. The critical roles of SpeB in early stage of infection have made them attractive targets for in vivo diagnosis and treatment. A molecular imaging probe could report their enzymatic activity would be extremely valuable in managing GAS caused infection. We have used the GAS system as a model to demonstrate the enzyme activation approach. The main goal of this aim is to show a SpeB sensitive peptide sequence which could potentially be used for GAS imaging and treatment. A peptide substrate sequence, AIKAGY, has been reported to be selective for SpeB.(*1*) We have applied this peptide sequence to prepare a SpeB specific imaging probe (Figure 1). Briefly, grafted D-polylysine copolymer (DPGC) was first functionalized by reacting iodoacetic anhydride with DPGC (1 mg, MW= 375 KDa) in basic condition, and then the prepared Iodoacetylated-DPGC was reacted with Cy5.5-peptide substrates (1 mg) in sodium acetate buffer (300 µl, 50 mM, pH 6.5) overnight at r.t in dark. The formed imaging probes were collected by membrane cutoff filtration (50KD) and quantified by measuring Cy5.5 molar absorbance at 681 nm. Peptide loadings on DPGC was calculated using the relative mole ratio of fluorochrome to DPGC. On average, 20-25 peptides were

attached to each DPGC molecule. The quenching efficiency (94%) of the probes was quantified by measuring the fluorescence signal intensity of imaging probes to that of free equal-moled Cy5.5 dye.

Since purified SpeB protease is not commercially available and repeated attempts to produce recombinant enzymatically active SpeB have been unsuccessful, we have used the bacterial culture supernatant from a wild-type strain (Strain I, MGAS10870) of GAS, and its isogenic mutant strains (ΔSpeB), lacking SpeB protease to perform the evaluation. In a GAS culture supernatant, SpeB constitutes ~80% of the total protein, so that the assays could be conducted conveniently. Probes (0.2 nmole) in 150 uL of PBS buffer were mixed with concentrated culture supernatant (50 µL, 5X concentration). At different intervals, the

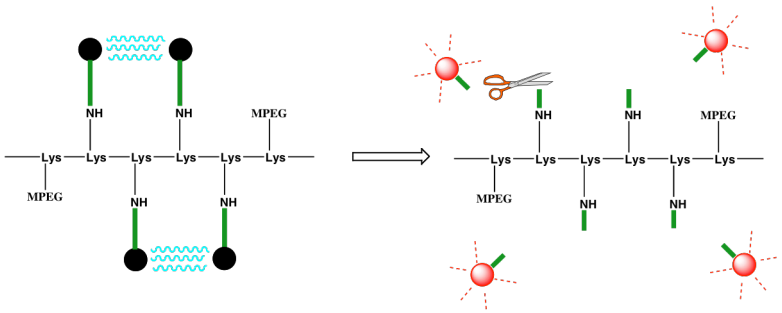

Figure 1: Schematic diagram of SpeB probe activation. Fluorochromes are covalently coupled to a polylysine backbone sterically protected by methoxy-polyethylene-glycol via a specific SpeB peptide substrate (green line). Due to the proximity of the fluorochromes, autoquenching occurs and no fluorescent signal can be detected in the non-activated state. After SpeB cleavage of the peptide spacer, fluorochromes are released from the carrier and become brightly fluorescent.

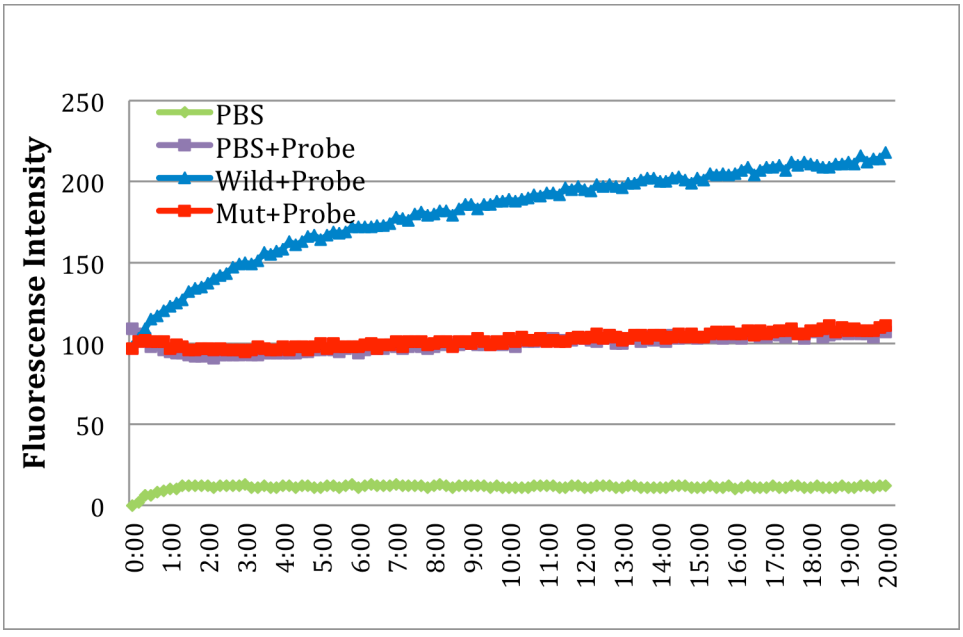

Figure 2: SpeB probe validation using a SpeB positive (Wild) and negative (Mut) GSA strain. The SpeB probe prepared in Aim 1 was incubated with GAS culture soup in PBS buffer for 20 hours. The fluorescent signal was measured by 680 nm excitation and 720 nm emission. The wild type strand with SpeB activity was able to active the probe, while the mutant strain without SpeB couldn't. The negative control also showed great stability of the probe in PBS.

fluorescence intensity was measured with 680 nm excitation and 720 nm emission using a computer-controlled fluorescence plate reader (Safire II, TECAN, Durham, NC). A negative control experiment was done with incubating the probe in PBS buffer only. As expected, the probes were activated by SpeB positive strain, but not by its isogenic mutant strain (Figure 2). The fluorescent signal was increased more than 100%. In addition, without cell culture soup, the probe remained stable in the PBS buffer. This result suggests that the reported SpeB peptide substrate could be an excellent sequence for our imaging probe preparation. More validation will be conducted during the next period to confirm the specificity of this peptide sequence.

The self-quenched SpeB imaging probe was then tested with different known GSA bacteria. Bacterial culture supernatants from a wild-type strain (Strain I, MGAS10870) of GAS, and its isogenic mutant strains, with different amount of SpeB protease, were collected for assays. Probes (0.2 nmole) in 150 uL of PBS buffer were mixed with concentrated culture supernatants (50 µL, 5X concentration). At different intervals, the fluorescence intensity was measured with 680 nm excitation and 720 nm emission using a computer-controlled fluorescence plate reader (Safire II, TECAN, Durham, NC). A negative control experiment was done with incubating the probe in PBS buffer only. As expected, the probes were activated by SpeB positive strains to different degree, but not by control strains (Figure 3). The fluorescent signal was increased more than 700%. In addition, without cell culture soup, the probe remained stable in the PBS buffer. And importantly, the intensity of fluorescent signal correlated well with the SpeB expression level. This result confirmed that the prepared SpeB peptide substrate is an excellent probe for SpeB imaging, and the activation concept is useful in imaging disease associated enzyme activity.

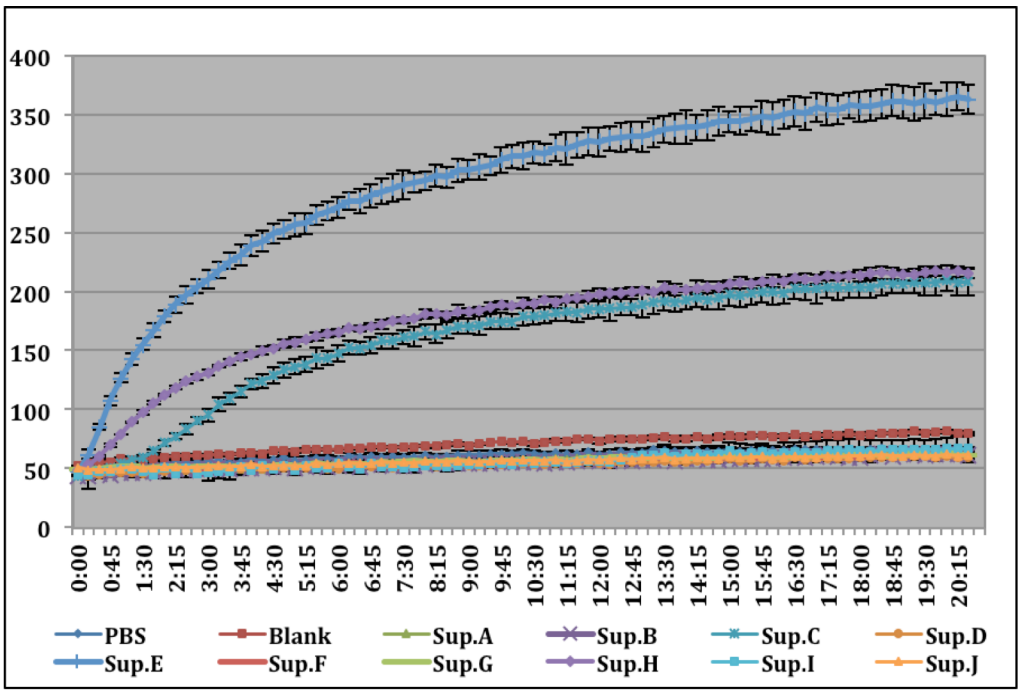

Figure 3: Activation of SpeB specific probe using the various GSA strands. It was confirmed that the GSA strand had highest fluorescent signal did express highest level of SpeB.

Aim 2: ESNM fabrication for maximum imaging sensitivity and drug loading capacity.

General assembling approach of ESNM

Layering fabrication technology is a gentle assembly procedure to add multiple layers of thin film onto a surface or a particle (Fig. 4).(*2*) The assembly is based on charge-charge interaction between positively and negatively charged polymers. Onto a core particle the first layer of charged polymer is added by electrostatic adsorption, and then an opposite charged polymer is added onto the first layer by charge-charge interaction. By repeating cycles of centrifugation and resuspension, multiple layers of polymers can be assembled conveniently. The thickness of the layers is controlled by repeating fabrication cycles.

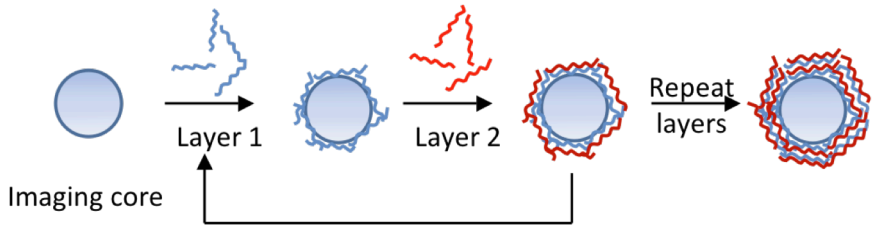

Figure 4: Schematic diagram of multiple-layer fabrication. Layer 1 and layer 2 have opposite overall charges.

Procedure of ESNM fabrication

To assemble the proposed ESNM nanoparticle, we have developed a formulation protocol using positively charged poly-L-Lysine (PLL, MW = 15,000-30,000 Da), and negatively charged double stranded DNA (Herring sperm, <50 bp in length) as the charge paired polyelectrolytes. Onto an inert gold particle core (42 nm), polylysine was first added. The zeta-potential and particle size were found to be +51mV and 44 nm, respectively, after the first layer. The particles were washed thoroughly with deionized water at least 3 times before the deposition of next layer. DNA solution was then added to the polylysine coated nanoparticle for 60 min. As expected, the surface charge was changed from +51 mV to -33 mV.

Three additional layers of polylysine and DNA were added sequentially following the same procedure. The alternative positive and negative zeta potential was indeed taking place when the outside surface was changed from polylysine and DNA (Fig. 5). The coating of each layer was confirmed by the changes of surface zeta potential. The particle size was increased from 40 nm to 208 nm after 5 layers of PLL and 4 layers of DNA. It was found that the particle size

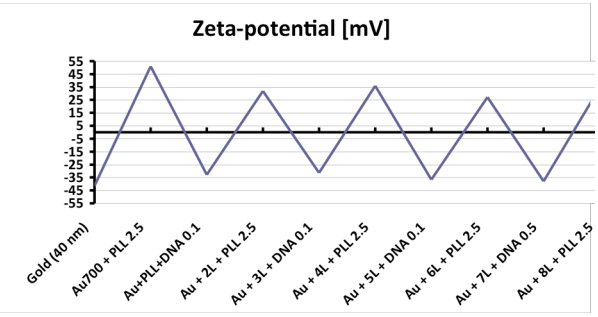

Figure 5. Surface zeta-potential of gold nanoparticle after alternate layers of polylysine or DNA.

could be adjusted by adding different amount of PLL or DNA.

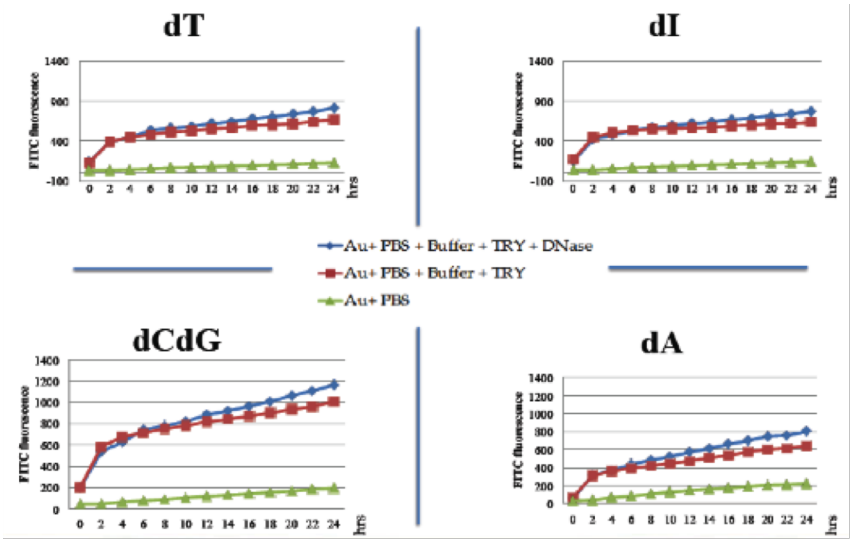

Figure 6: in vitro activation of ESNM using trypsin and DNase 1. Poly dCdG complex give the highest activation and fastest kinetics.

Using this developed protocol, we prepared ESNM particles with five different types of single stranded nucleic acids, including polydeoxyadenylate (poly-dA), polydeoxythymidylate (poly-dT), polydeoxyinosinate (poly-dI) polydeoxycytidylate (poly-dC) Polydeoxygunaylic acid – polydeoxycytidylic acid (dC-dG). All particles were characterized as with double stranded model DNA, and their properties were indeed similar. The prepared particles were then treated with DNase 1 and trypsin to measure the release kinetics (Figure 6). Trypsin was required in this assay, because PLL was the positive component of the ESNM. The release of the fluorescent signal was measured using an automatic fluorescent plate reader. It was found that the dCdG gave the best kinetics during the 24 hours period. However, the contribution of DNase was not significant in all tested groups, suggesting PLL is the key component in holding all layers together.

Formulation of enzyme activatable imaging nanoparticle

Using the developed fabrication protocol, a novel type od ESNM was designed for enzyme imaging. In this formulation, the negatively charged polyelectrolyte used was polyacrylic acid (PAA), and the positively charged layer was PLL decorated with fluorescein isothiocyanate (FITC). Because the positively charged lysine residues in PLL can be degraded by many intracellular proteases, such as cathepsins B and L, PLL was selected as the backbone to provide a slow-release capability. When multiple FITC residues were loaded onto one PLL backbone, self-quenching occurred due to the close proximity of neighboring fluorochromes. Importantly, the quenched signal could be recovered after proteolytic degradation of the PLL backbone. The optimal loading ratio that provided a 34-fold signal amplification was found to be FITC/PLL = 10/1 (Figure 7). Importantly, when the protease degradable PLL was replaced with protease non-degradable PDL, the added protease couldn't change the fluorescence signal.

To assemble the multilayered fluorescent ESNM, the negatively charged AuNPs (40 nm) in water were dropped into the positively charged PLL-FITC solution (average Mw = 50 kDa) for the first layer of coating. The reaction mixture was incubated for 30 min, and then the coated particles were spun down by centrifugation. After three washes with sterilized water, the PLL-FITC-coated AuNPs (1L AuNPs) were added to the negatively charged PAA (Mw = 15 kDa) solution. By repeating these procedures, multilayered AuNPs – up to five layers of PLL-FITC and four layers of PAA (5L AuNPs) – were successfully fabricated by electrostatic interactions. The hydrodynamic diameter of the prepared AuNPs was measured by dynamic light scattering (DLS) after coating with each layer. The size of initial bare AuNPs was 40 nm and the prepared particle size increased steadily with the number of layers (1L: 63 nm; 3L: 112 nm; 5L: 144 nm) (Figure 8a). When treated with protease, the fluorescence signal change was layer-dependent. The optimal formulation was 5L AuNPs (five layers of PLL and four layers of PAA), the fluorescence of which changed by 195-fold. The fluorescence signal change of 7L AuNPs, however, was similar to that of 5L AuNPs despite the two additional layers of PLL-FITC added to the particles (Figure 8b).

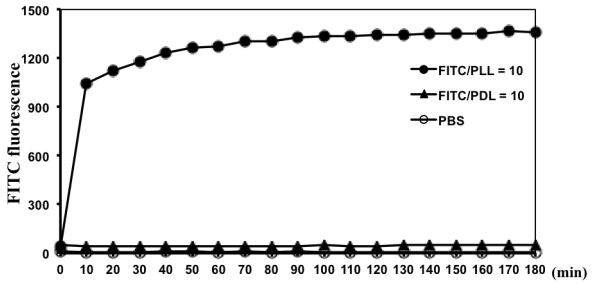

Figure 7. Protease-assisted cleavage of PLL or PDL conjugated with FITC. After incubation of PLL-FITC or PDL-FITC with or without trypsin in PBS, the fluorescence intensity was examined for 3 h.

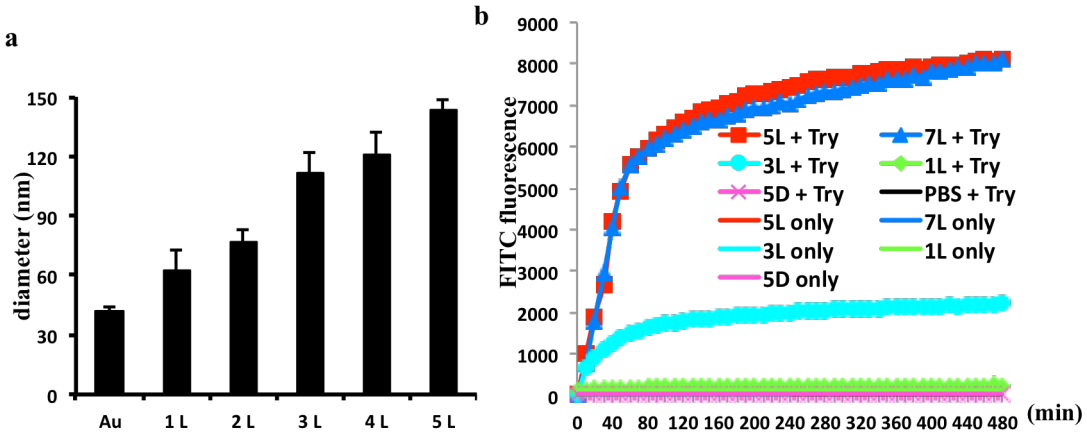

Figure 8: Characterization of ESNM. (a) Diameter of bare AuNPs and polyelectrolyte-coated AuNPs. (b) Protease-assisted fluorescence release from various AuNPs. Multilayered fluorescent AuNPs were incubated with or without trypsin in PBS and the fluorescence intensity was examined to 8 h.

Formulation of bifunctional ESNM for cell viability imaging

The nanoprobe for cell viability imaging was prepared by assembling multiple layers of polyelectrolytes on an inert AuNP, based on charge-charge interaction (Figure 9). The negatively charge layers are PAA and the positively charged layers are a biodegradable poly-L-lysine (PLL) tagged with cy5.5 as a live cells reporter, and/or a poly-D-lysine (PDL) labeled with fluorescein isothiocyanate (FITC) as a dying cell reporter. Because the positively charged PLL can be degraded by many intracellular proteases, such as cathepsins B and L, while PDL can only be degraded under severe circumstance, such as apoptosis and necrosis.

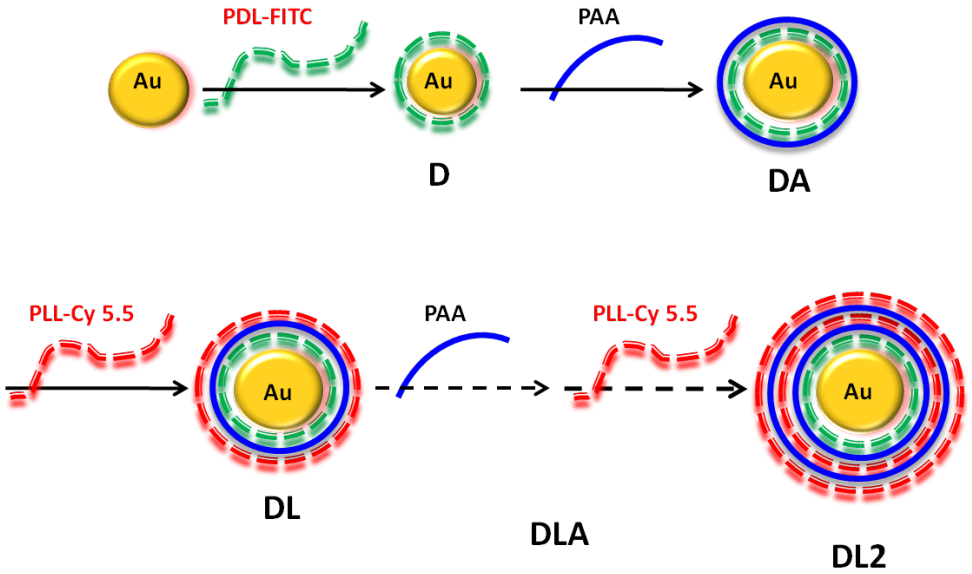

Figure 9. Preparation process for multilayered nanoprobe using PDL-FITC / PLL-cy5.5 and PAA as the charged polyelectrolytes.

Optimization of L3 nanoparticle: A series of PLL-Cy5.5 (PLL-C) was prepared by reacting PLL (0.2 mg) with different amount of cy5.5 (0.0125, 0.025, 0.05, 0.1, or 0.2 mg) in $NaHCO_3$ (1 mM, 100 μL) in the dark at room temperature for 30 min. The reaction products were separated using molecular-weight-cutoff membrane filters (10 kDa). The resulting PLL-C were collected and washed several times with sterilized water until all free dye was removed. To measure the quenching/dequenching effect, the prepared PLL-C (0.2 nmol in 5 μL) in PBS was incubated with trypsin–ethylenediamine tetraacetic acid (EDTA; 10 μL, 0.25%) in a 96-well culture plate at 37 °C, and the increase in the cy5.5 fluorescence signal was assessed using a fluorescent plate reader with 665 nm excitation and 700 nm emission for 15 h. According to the changes of the fluorescence intensity, the optimal loading was determined to be PLL-C7 which had 7 cy5.5 molecules per PLL molecule (Figure 10a). A greater than 6-fold change in fluorescence signal was observed. PLL-C6 with 6 Cy5.5 showed 3 fold increase in fluorescent intensity. While other PLL with lower loading, such as PLL-C3, PLL-C2 and PLL-C1, all suffered from poor dequenching effect.

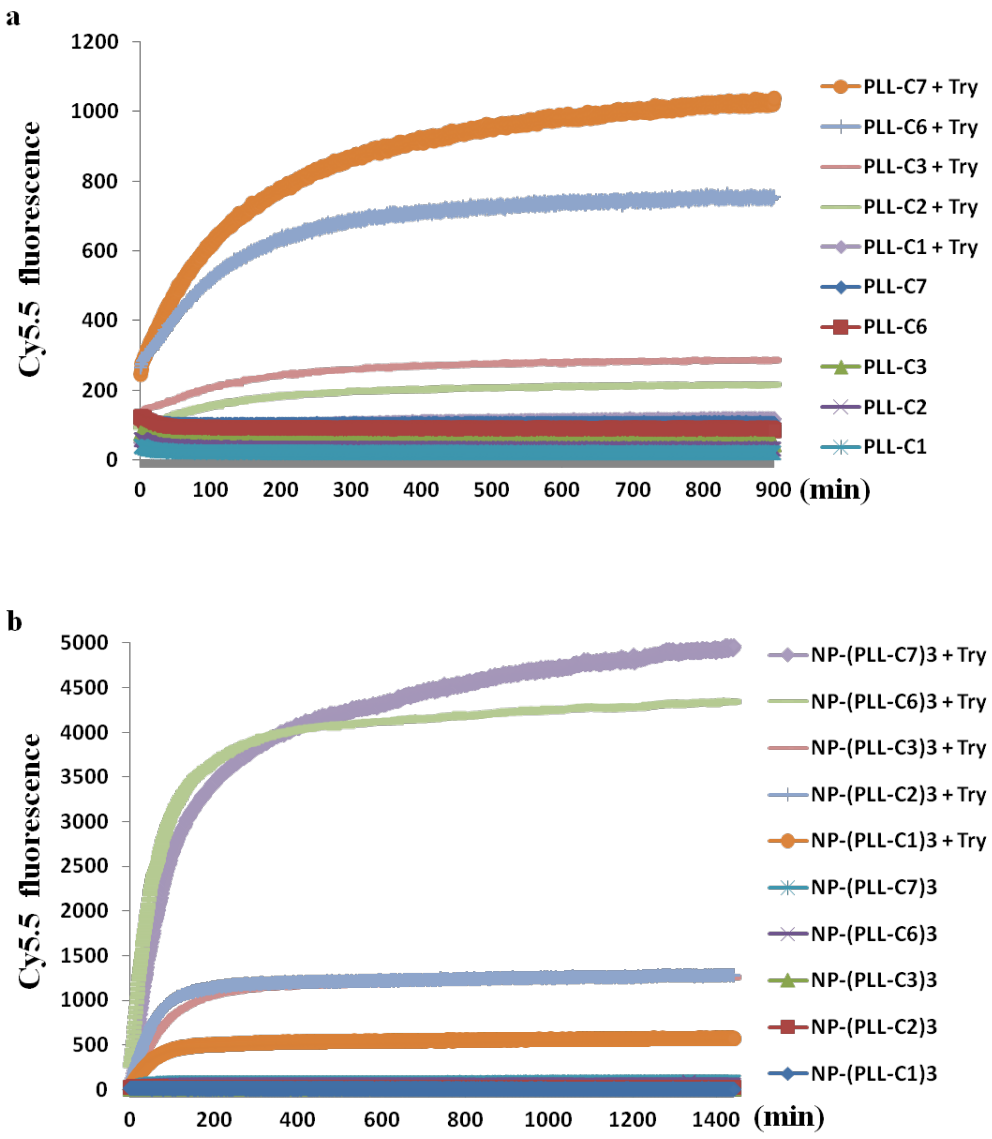

Figure 10. Protease-assisted cy5.5 release from PLL conjugated with different concentration of cy5.5 (a) or three layers of PLL-cy5.5 coated NPs (b). After incubation of different concentration of PLL-cy5.5 (a) or NP-(PLL-C)3 (b) with or without trypsin in PBS, the fluorescence intensity was examined until 15 h or 24 h.

To further confirm the activation effect, all PLL-C were used to prepare nanoprobes. AuNP solution (40 nm, 3.15×10^9 particles in 700 μL) was added dropwisely to a PLL-C solution (PLL, 1.8 nmol in 500 μL). After incubating for 30 min in the dark with gentle shaking, the solution was centrifuged (30 min at 16,100 g) and the supernatant was collected. After a further wash, the gel-like deep blue pellet were added to the polyacrylic acid (PAA) solution (23.3 mM , 500 μL). The reaction solution was kept in the dark for 30 min with gentle shaking, followed by three washes. The deposition procedures were repeated twice with PLL-C layers. The prepared particles were then treated with trypsin

to measure the activation. As shown in Figure 2b, particles were stable in phosphate buffered saline (PBS), but when treated with protease the fluorescence signal increased. The optimal formulations with 256-fold increases were NP(PLL-C6)3 and NP(PLL-C7)3. Other formulations offered much smaller changes.

Preparation of D3 and DL2nanoparticles: The D3 and DL2 nanoparticles with 3 layers of PDL-FITC, and one layer of PDL-FITC/2 layers of PLL-C6 were prepared using the same protocol.

Preparation of therapeutic ESNM

To prepare the multilayered siRNA-coated AuNPs (sRAuNPs) which have long-lasting controlled release and gene silencing effects, we have developed a fabrication method to prepare multilayer siRNA delivery system (Figure 11). The negatively charged AuNPs (size: 40 nm) in water were dropped into the positively charged poly-L-lysine (PLL) solution (average Mw = 22.5 KDa). After a 30-min incubation at room temperature with shaking and several washes with sterilized water, the positively charged PLL-coated AuNPs were added to the negatively charged siRNA solution. After incubation, free unbound siRNAs were removed by centrifugation and an additional PLL layer was added so the resulting positively charged AuNPs (sR1P) had one layer of siRNA and two layers of PLL. By repeating this procedure again, AuNPs (sR2P) with two layers of siRNA and three layers of PLL were successfully fabricated by electrostatic interactions. A zigzag pattern of the surface zeta-potential of each layer supported the success of the layering (Figure 12). The final particle size, determined by dynamic light scattering (DLS) measurement, was found to be approximately 150 nm (Figure 12).

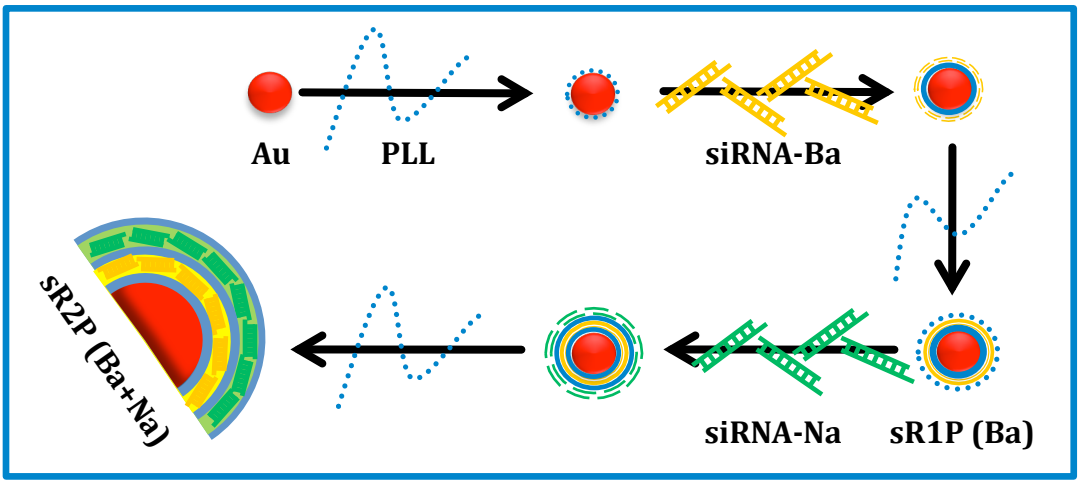

Figure 11: The process of preparing multilayered siRNA-coated AuNPs by electrostatic interaction.

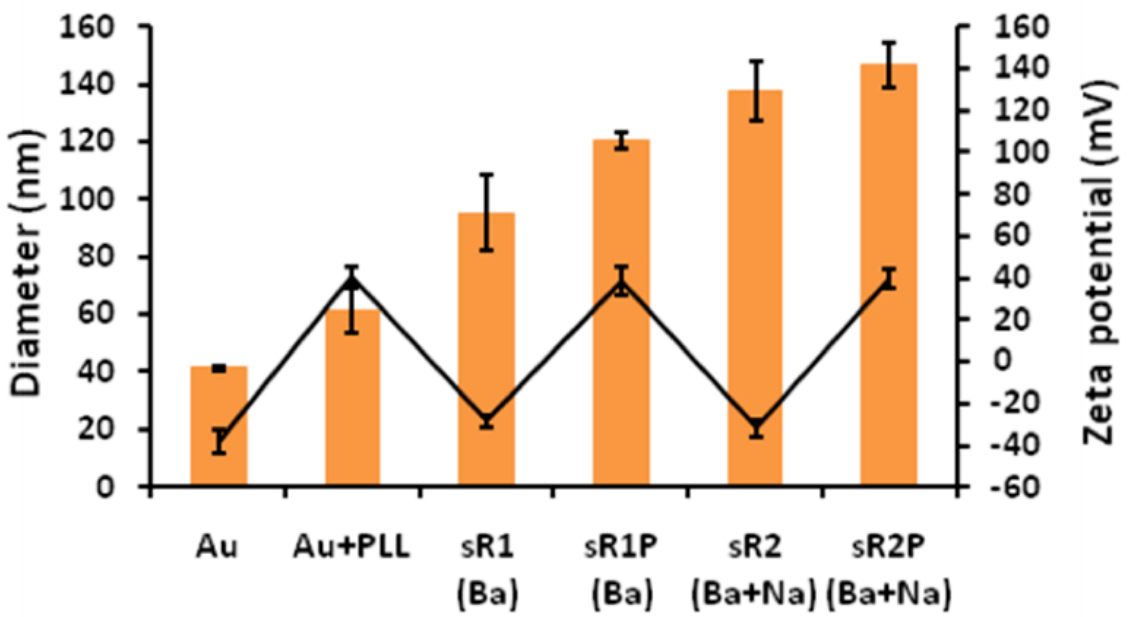

Figure 12: The average size (orange bar) and zeta potential (black circle) of multilayered sRAuNPs.

Fabrication of the targeting ESNM

To add a targeting capability to the previously developed siRNA delivery system. To achieve this goal, we have developed a fabrication method to prepare multilayer siRNA delivery system with a surface coating of targeting polymer (Figure 13). Hyaluronic acid (HA) is a naturally occurring liner polysaccharide in the body which is biodegradable, cytocompatible, nontoxic, and nonimmunogenic. It has high affinity to the cell surface adhesion molecule CD44 which interacts with other ligands, such as osteopontin, collagens, and matrix metalloproteinases (MMPs). It has been intensively investigated for HA-specific drug delivery system *via* CD44-mediated endocytosis due to its polyanionic characteristics and negligible nonspecific interaction with serum components. CD44 also has been identified as the determinant of progression to the metastatic breast cancer because it is rarely found in healthy tissue but is highly expressed in tumor cells with metastatic pheonotype. Taking advantage of the negatively charged HA, the CD44 targeting particles were packed using the developed layering technology. The siRNA containing nanomedicines were first prepared as previously described. After the last cycle, HA (Average Mw = 50 KDa) was added to the particle and the surface charge was converted from the positive to negative quickly (Figure 14). Zigzag pattern of the surface zeta-potential of each layer supported the success of the layering. The final particle size, determined by dynamic light scattering (DLS) measurement, was found to be approximately 100 nm (Figure 14).

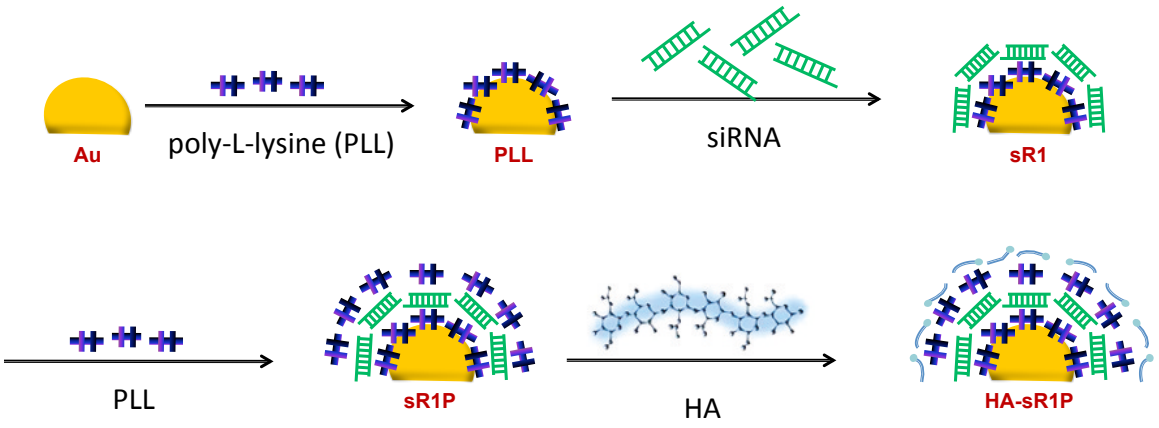

Figure 13: The electrostatic assembling process of preparing multilayered siRNA-coated AuNPs for targeted delivery.

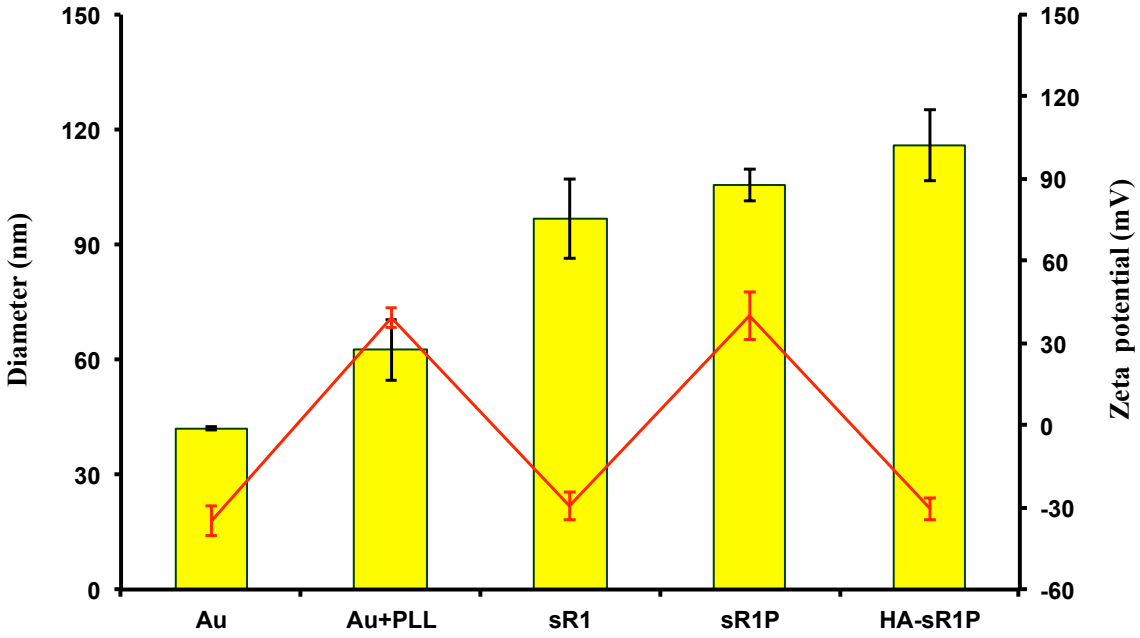

Figure 14: The average size (yellow bar) and zeta potential (red line) of multilayered HA-sR1P which has one layer of PLL, one layer of siRNA, one layer of PLL and then one more layer of targeting HA.

Aim 3: To demonstrate the imaging and therapeutic efficacy of ESNM in biological models.

Long-term cell imaging

The usage ESNM to image live cells was investigated by comparing the nanoprobe with commercially available cell labeling reagents CMTMR using fluorescence microscopy. When incubated with CMTMR, the fluorescence signal was strong at short time points but decreased quickly and lasted only for 2 days. However, a prolonged fluorescence signal was found with 5L AuNPs. A high fluorescence signal was maintained for more than 14 days with negligible background. To investigate the sub-localization of multilayered nanoprobes, HeLa cells were stained with Hoechst and LysoTracker after treatment with 5L AuNPs (Figure 15). Merged fluorescence signal of FITC and LysoTracker clearly showed the lysosomal delivery of multilayered fluorescent nanoprobes. Two hours after incubation, the merged image of FITC and LysoTracker signals in some cells showed significant overlapping, indicating the particles were located

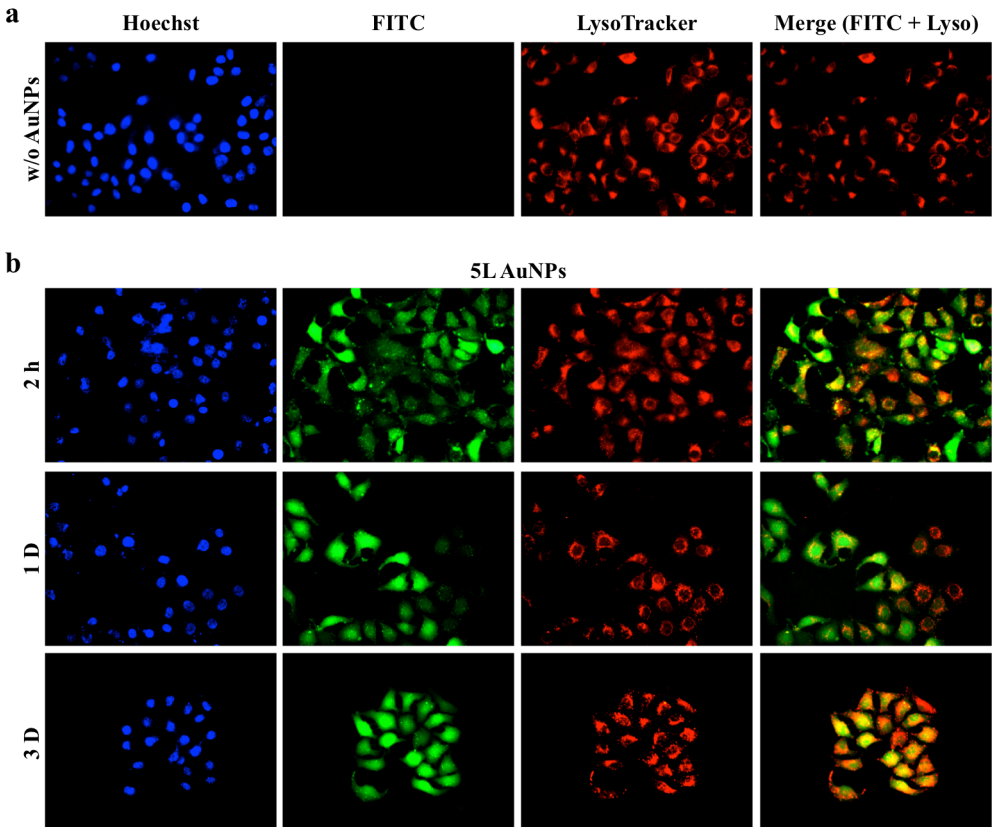

Figure 15. Subcellular localization of the multilayered ESNM. HeLa cells were incubated without (a) or with (b) 5L AuNPs (FITC 2.7 nmole) for 12 h and washed three times with PBS. At each time point (2 h, 1 day and 3 day), cells were stained with LysoTracker (1 mM) for 1 h, Hoechst (1 mM) for 5 min and then fluorescence signal was investigated with fluorescence microscopy (magnification : 40 X) using different filter sets (Hoechst : blue / 5L AuNPs : green / LysoTracker : red).

and activated in lysosomes. While in some other cells, FITC fluorescent signal was distributed evenly in whole cells. It suggested that somehow the nanoprobes could flee the lysosomes. At day 3, high FITC signal was found in nucleus. Further supported the hypothesis that the particles were able to escape from lysosomes and continued to release fluorescent signals.

To gain a better understanding of signal retention after cell division, a suspension of the Jurkat T cell line was tested with 5L AuNPs (Figure 16a) or the commercially available cell tracking agents, CM-DiI and CMTMR (Figure 16b,c). After incubation with various labels, aliquots of cells were collected and analyzed by flow cytometry (Figure 17). The initial fluorescence intensity of each label was controlled to a similar level for a fair comparison. Similar retention patterns were seen with the CM-DiI and CMTMR cell trackers. The intensity in CM-DiI- and CMTMR-treated cells had declined to 8 % and 3 % of the original intensity, respectively, after 4 days of incubation. At day 7, the labels were largely gone, and the signal had declined to a background level. As the doubling time of the Jurkat T cell line is approximately 48 h, this result suggested the label lasted for about three divisions. In contrast, the 5L AuNPs offered a much longer signal duration. At day 4, the signal intensity was still 24 %. At days 7 and 14, the signal had declined to 12 % and 7 %, respectively. Even after 21 days, the 4 % remaining signal was still detectable by FACS. These results suggest that the slow release mechanism prolonged the duration of action of the cell labels and that the ESNM are suitable for labeling dividing cells.

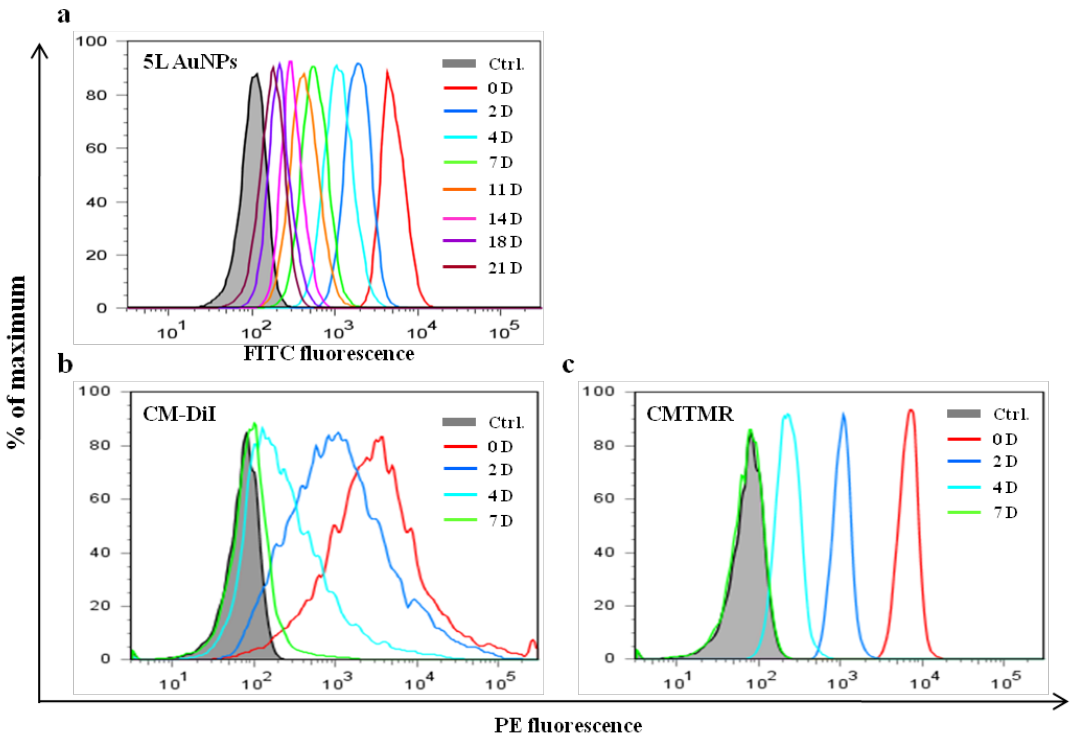

Figure 16. Fluorescence retention through generations in Jurkat cells. After treatment with 5L AuNPs (FITC 13.6 nmole), CM-DiI (1 μM), or CMTMR (2 μM), fluorescence intensity was evaluated by flow cytometry (a-c) for 21 days.

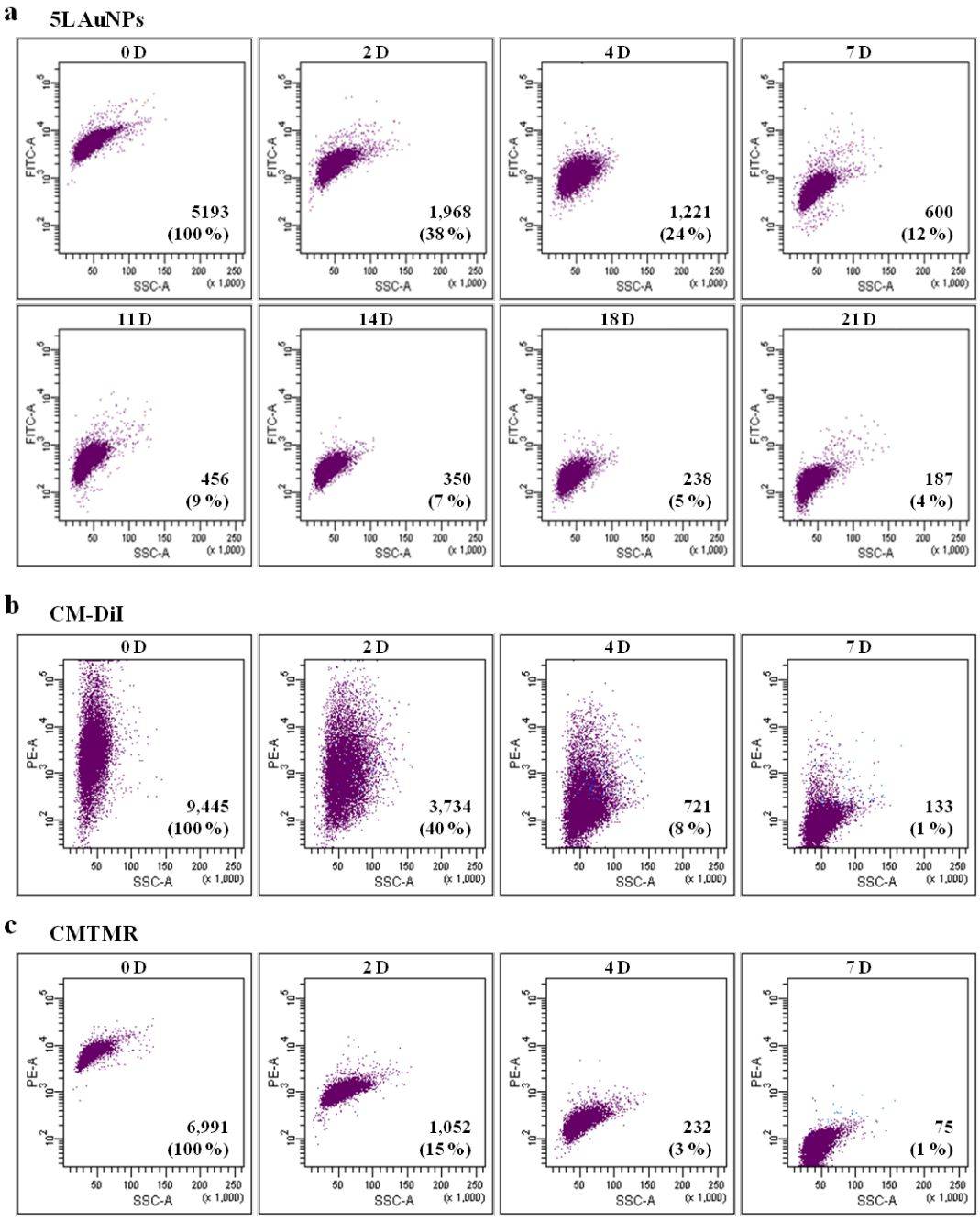

Figure 17. Cell population and fluorescence intensity of Jurkat cells. After treatment with 5L AuNPs (FITC 13.6 nmole) (a), CM-DiI, 1 mM (b) or CMTMR, 2 mM (c) to Jurkat cells, fluorescence intensity was measured by flow cytometry with time course. Inserted number in each column shows the average fluorescence intensity value and the percentage, the intensity at 0 Day was set as 100 %.

Bifuncational ESNM for cell viability imaging.

The ability of D3 (three layers of PDL-FITC) nanoparticle to sense apoptosis was investigated by comparing the images of healthy and apoptotic cells. MDA-MD231 breast cancer cells were labeled with D3 NP for 12 hr, and then a commercially available apoptosis reporter, Annexin V-cy3, was added to the cells. After washes, the cells were monitored under FITC (green) and cy3 (Red) channel. As expected, cells are healthy and happy, therefore D3 nanoprobe remained silent and Annexin V stain was also negative (Figure 18a). While cells were treated with an apoptosis inducer, staurosporine, fluorescent signal was observed in both FITC and cy3 channel (Figure 18b). The cy3 signal caused by Annexin V indicated an early event of apoptosis -- externalization of phosphatidylserine (PS). Importantly, fluorescent signal generated by D3 NP was also seen in cy3 positive cells, suggesting that D3 NP was activated under apoptotic condition, but silent in normal healthy cells.

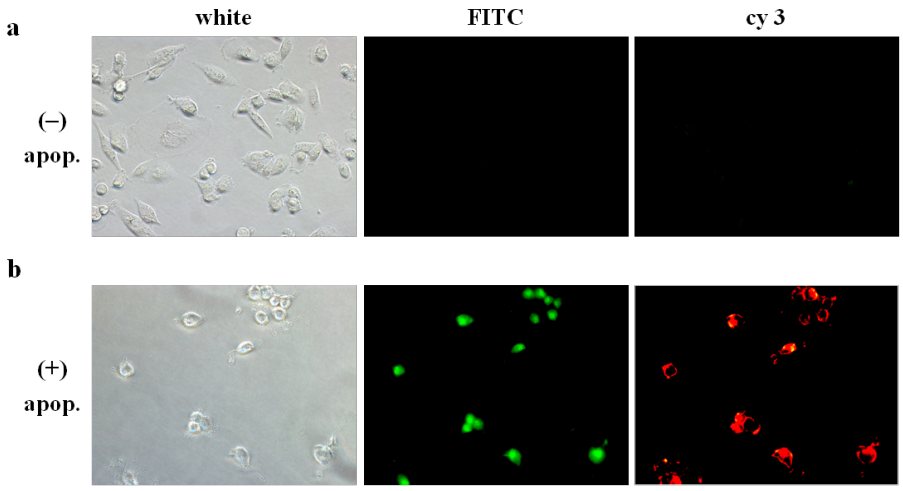

Figure 18. Apoptotic cell imaging with D3 NPs and Annexin V-cy3 in MDA-MB231 cells. After incubation for 12 h with D3, cells were stained with Annexin V-cy3 after washing with PBS. Fluorescence signal were assessed using fluorescence microscopy (magnification: 40 X) (a) without or (b) with apoptosis induction with staurosporine (4 mM) for 4 h.

Based on our design, all layers with optimized number of fluorochromes are optically silent (quenched). The fluorescent signal can only be seen when it is degraded (dequenched). PLL-C6 is consisted of normal Poly-L-lysine, so that several intracellular proteases, such as cathepsin B and L, could degraded it. While PDL-FITC is consisted of unusual Poly-D-lysine, most proteases cannot hydrolyze it. The previous experimental results showed that under the extreme condition, i.e. dying, PDL was degraded quickly (Figure 18b). Therefore a new nanoprobe was designed to report the viability of the cells. The DL2 NPs have one inner layer of PDL-FITC and two outer layers of PLL-C6, assuming the PLL outer layers will report the normal condition, and the PDL inner layer will report the apoptosis, if it happened. MDA-MB231 cells were treated with DL2 NP.

Without inducing apoptosis, only red signal (PLL-C6 degradation) was observed in all healthy cells (Figure 19a). No green signal (dying cells) was seen even after 4 days of incubation in normal media. However, immediately after apoptosis induction, green apoptosis signal was seen (Figure 19b). In comparison, D3 NPs, which only have PDL-FITC, showed no cy5.5 signal as expected. These results support our hypothesis that the hybrid NPs could report cell viability in real time. This type of viability imaging probe would be very useful in tracking cell therapy, and evaluating anticancer treatment effect.

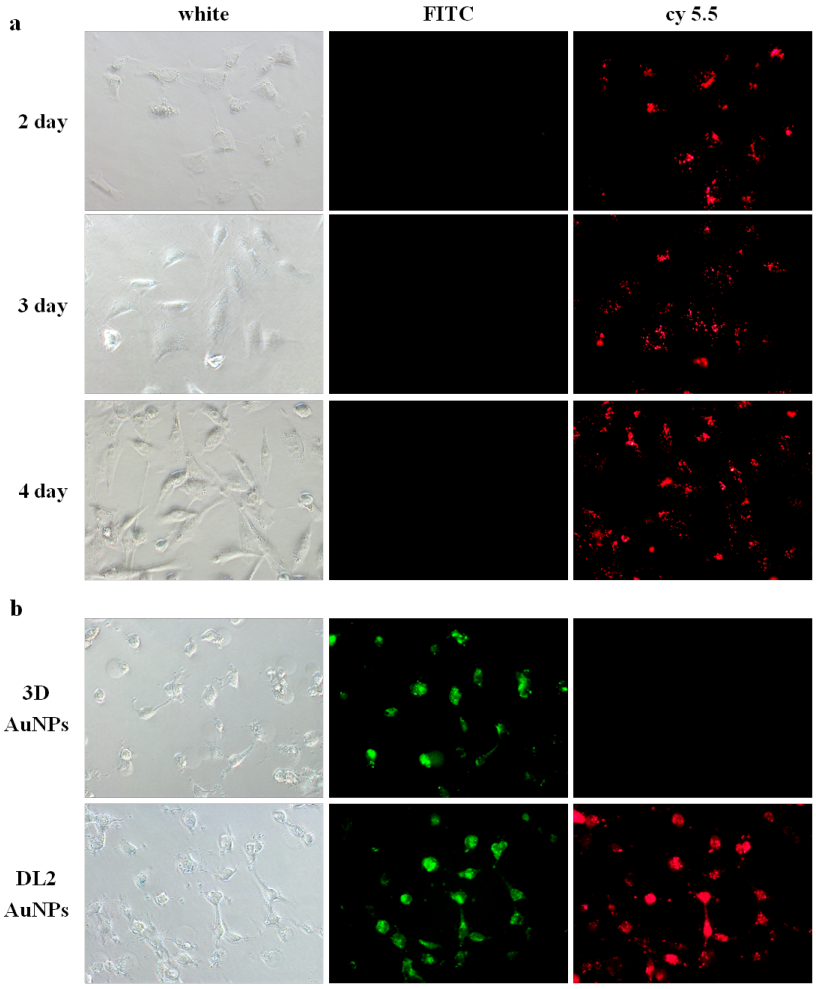

Figure 19. Viability imaging with DL2 NP and D3. MDA-MB231 cells incubated with DL2 NPs for 12 hrs, washed, cultured for 4 d, and then fluorescence images were acquired using FITC and cy5.5 filters (a). At day 4, cells were incubated with 4 mM of staurosporine for 4 h to induce apoptosis and imaged. A separate well of cells were treated the same but with D3 NP (b).

The gene silencing efficacy of ESNM in biological models.

Short interfering RNAs (siRNAs)-mediated gene regulation in mammalian cells was first discovered about two decades ago and siRNA has since shown immense potential in treating various diseases by silencing abnormally up-regulated genes. However, delivering the highly charged siRNA to the targeted cells and enabling the specific target gene silencing effect to persist remains challenging. To obtain a consistent silencing effect in vivo, it usually requires repetitive administration of the agent. However, such repeated injections have resulted in a substantial impediment to patient treatment, as evidenced by decreased enrollment in clinical trials and decreased patient compliance. Complete and prolonged gene silencing with a single treatment would offer enormous benefits for chronic diseases, scaling down the administration frequency in dosing schedule.

Two reported siRNA sequences, termed siLuc-Na and siLuc-Ba, against two different regions of the luciferase gene were used because maximal gene silencing effect has been reported with simultaneously applied multiple siRNAs. sRAuNPs were fabricated with one or two siRNAs. sR2P (Ba + Na) was prepared with siLuc-Ba on the first layer and siLuc-Na on the second layer, and the order of siRNA in sR2P(Na + Ba) was reversed. A scramble siRNA (siLuc-Sc), which has the same length but randomly sequenced of siLuc-Na, was included as a negative control.

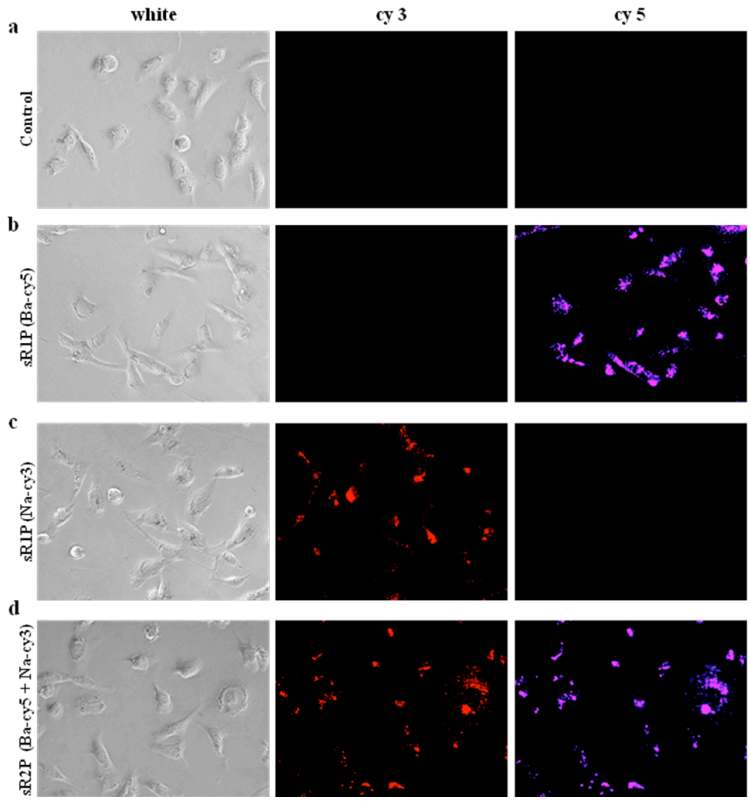

Figure 20. Cellular uptake of multilayered sRAuNPs. Images of released siRNA from various sRAuNPs were visualized using fluorescence microscopy with different filters after 24 h incubation in the absence (a) or presence of sR1P (Ba-cy5) (b), sR1P (Na-cy3) (c), and sR2P (Ba-cy5 + Na-cy3) (d) in MDA-MB231-luc2 cells.

To demonstrate the success of packing and intracellular delivery of sRAuNPs, the two siRNAs, siLuc-Ba and siLuc-Na, were labeled with cy5 and cy3 fluorescent reporters, respectively. Various sRAuNPs (1.58×10^8 particles), including sR1P (Ba-cy5), sR1P (Na-cy3), and sR2P (Ba-cy5 + Na-cy3), were incubated for 24 h with MDA-MB231-luc2 cells. The presence of siRNA in cells was investigated using fluorescence microscopy (Figure 20). Because a cy3 or cy5 reporter was anchored to each siRNA, the fluorescence images using cy3 and/or cy5 channels reveal the location of the released siRNA. We observed a spotty fluorescence signal diffused into the cytoplasm (Figure 20b-d). The images of both cy5 and cy3 fluorescence signals after treatment with sR2P (Ba + Na) clearly indicated the presence of two kinds of siRNA (Figure 20d). These cellular-uptake data indicate that sRAuNPs enter cells without a transfection agent. Once they are internalized, the siRNA could be freed from the particles by intracellular proteolysis.

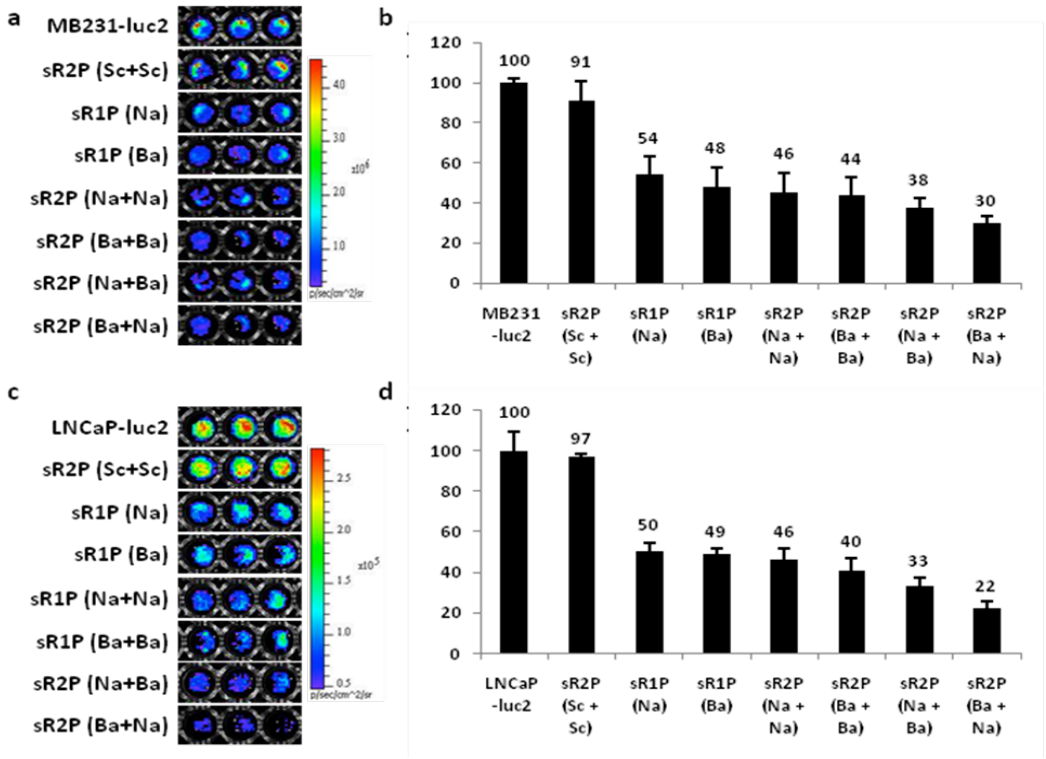

Figure 21. *In vitro* gene-silencing effect of multilayered sRAuNPs. The luminescence signal and the luminescence intensity (photons s^{-1}) in MDA-MB231-luc2 cells (a, b) or LNCap-luc2 (c, d) after incubation for 2 days with various sRAuNPs. The luminescence intensity of each cell line without treatment was set as 100 %. The results are representative of three independent experiments.

An initial gene-silencing screening experiment was performed by incubating MDA-MB231-luc2 cells with sR1P (Na), sR1P (Ba), sR2P (Na + Na), sR2P (Ba + Ba), sR2P (Na + Ba), and sR2P (Ba + Na) for 2 days (Figure 21a, b). A control sR2P prepared with two layers of scrambled siRNA, termed as sR2P (Sc + Sc), was also used as a negative specificity control. After incubation, the particles were washed away, and MDA-MB231-luc2 cell luminescence was measured immediately after addition of luciferin. It was

determined that the luminescence was decreased to approximately 54 % by sR1P (Na) (siLuc-Na 0.2 nmole; 1.58×10^8 particles) and 48 % by sR1P (Ba) (siLuc-Ba 0.2 nmole; 1.58×10^8 particles) when the luminescence of untreated cells was set as 100 %. With the same number of particles (1.58×10^8), the luminescence intensities of sR2P (Na + Na), sR2P (Ba + Ba), sR2P (Na + Ba), and sR2P (Ba + Na) were reduced to 46 %, 44 %, 38 %, and 30 %, respectively. As shown in Figure 4c and d, similar results were observed with LNCaP-luc2 cell lines (sR1P (Na) : 50 % / sR1P (Ba) : 49 % / sR2P (Na + Na) : 46 % / sR2P (Ba + Ba) : 40 % / sR2P (Na + Ba) : 33 % / sR2P (Ba + Na) : 22 %). When the specific siRNA was replaced with the scrambled siRNA (total siLuc-Sc 0.4 nmole), the silencing effect was insignificant. These data reveal the sequence specific silencing effect of the luciferase gene in two different cancer cell lines and show both sequences have similar inhibition effects.

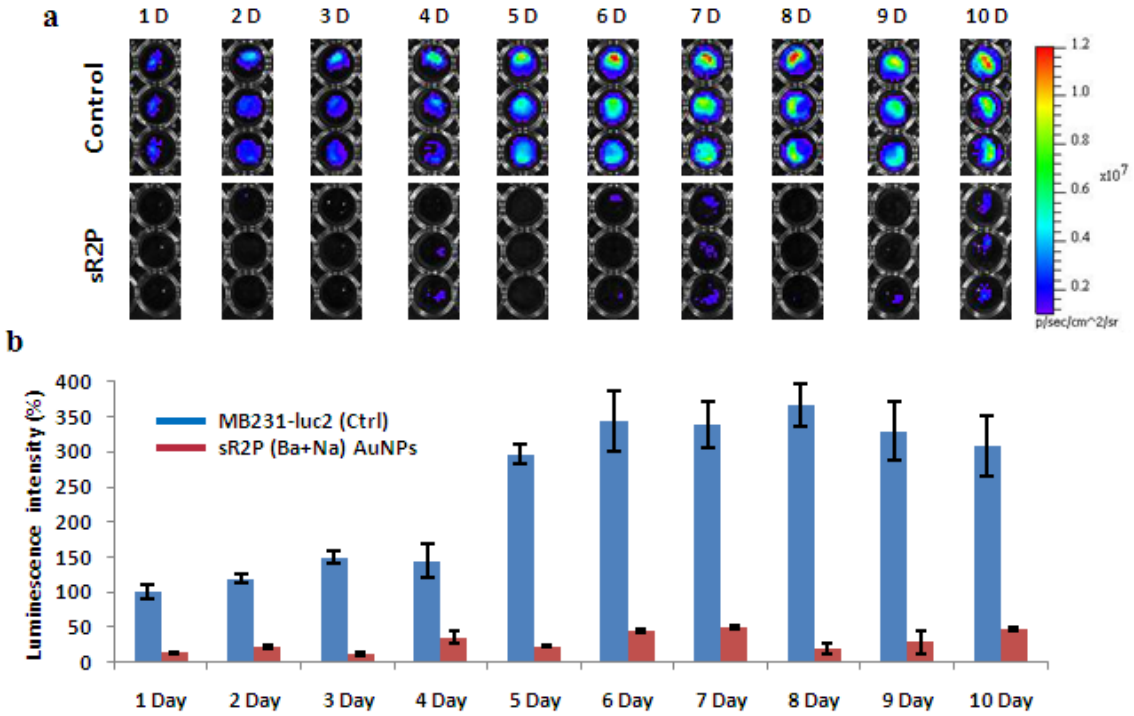

Figure 22. Prolonged gene-silencing effect of multilayered sRAuNPs. (a, b) The prolonged gene silencing effect was also evaluated by measuring the luminescence signal for up to 10 days after treatment with sR2P (Ba + Na) in MDA-MB231-luc2 cells. The luminescence intensity without treatment at day 1 was set as 100%. The results are representative of three independent experiments.

MDA-MB231-luc2 cells were treated for 2 days with sR2P (Ba + Na) in a 6-well plate (each siRNA 2.0 nmole; 1.58×10^9 particles). The cells were washed and aliquoted into separate 96-well plates for the time course study (up to 10 days). As shown in Figure 22a and b, the efficiency of gene silencing after treatment with sR2P (Ba + Na) on day 1 was 14 % when the initial luminescent intensity of control cells was set as 100 %. This significant gene silencing effect was sustained for at least 10 days (48 %). In contrast, the luminescent signal increased with time as the control untreated cells divided. The

luminescent signal of the untreated cells was approximately 400 %, but the signal of the treated cells was less than 50 % of the original signal. The experiment was forced to end at day 10, because of the physical constraint of the wells.

Although toxicity of surface modified AuNPs decorated with other polycationic polymers has been reported, cytotoxicity of the prepared particles was not observed. As shown in Figure 23, no significant toxicity was detected in any sR1P or sR2P-treated MDA-MB231-luc2 or LNCaP-luc2 cells, indicating silencing of the luciferase gene does not cause of non-specific cytotoxicity. In contrast, some toxicity was observed with Lipofectamine 2000 in both cell lines and less than 80 % cells were viable.

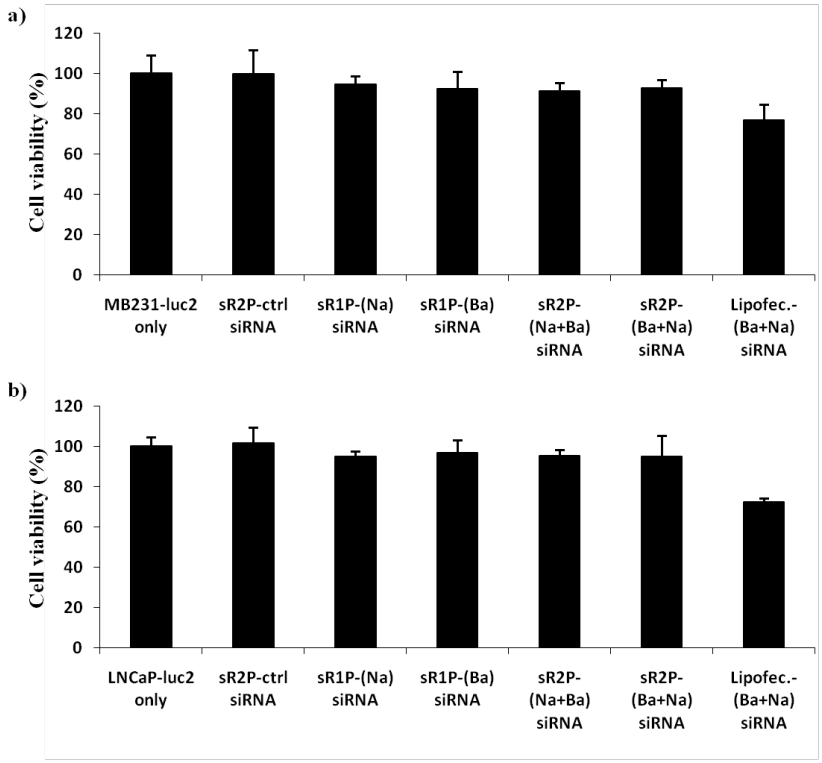

Figure 23. Cytotoxicity of multilayered sRAuNPs. Cell viability was evaluated after treatment with various multilayerd sRAuNPs or Lipofectamine 2000 using CellTiter solution in (a) MDA-MB231-luc2 and (b) LNCaP-luc2 cell lines. Results are representative of three independent experiments.

Targeted ESNM in cell culture

To validate the cell targeting efficiency, particles sR1P, which contain siRNA against luciferase, with or without HA layer were prepared. The siRNA was label with a fluorochrome, cy3, for easy tracking. Three breast cancer cell lines, MDA-MB231, MDA-MB436 and MCF-7, with different amount of CD44 were chosen for this delivery study. The prepared particles (1.58×10^8 particles), including sR1P, and HA-sR1P, were incubated for 24 h with cells. The presence of siRNA in cells was investigated using fluorescence microscopy (Figure 24). Because a cy3 reporter was anchored to each

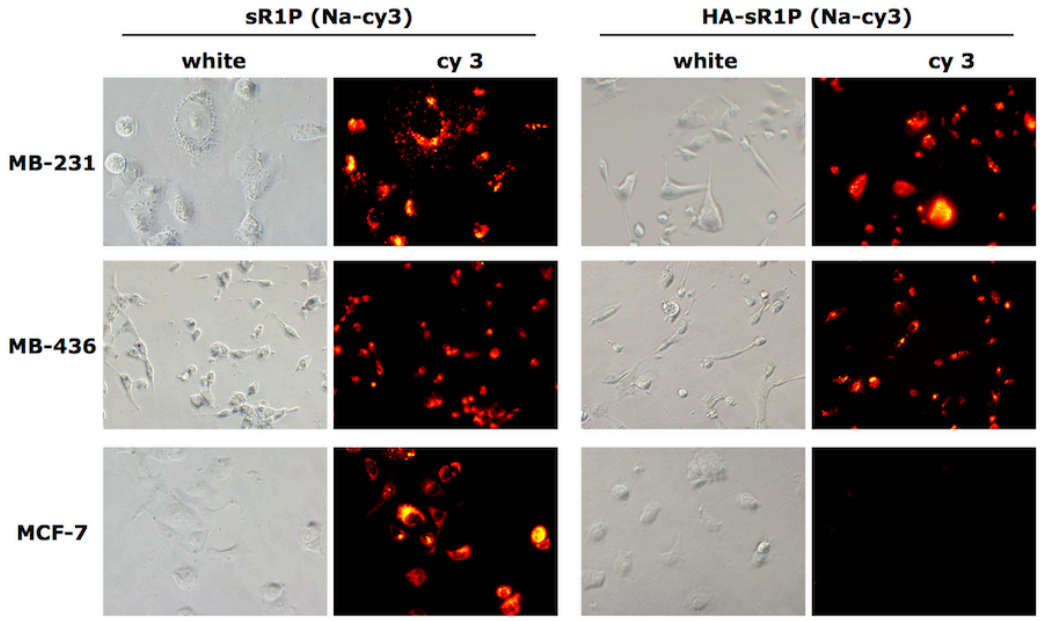

Figure 24. Cellular uptake of sR1P with (Right) or without HA (Left) coating. Images of released siRNA from various particles were visualized using fluorescence microscopy after 24 h incubation in MDA-MB231 (CD44+), MDA-MB436 (CD44+), and MCF-7 (CD44-) cells.

siRNA, the fluorescence images reveal the location of the released siRNA. We observed a spotty fluorescence signal diffused into the cytoplasm. As expected, HA-sR1P only labels the high CD44 expressing cells (MDA-MB231, MDA-MB436), not the low CD44 expressing cells (MCF-7). Interesting, different from the HA-sR1P treated cells, the siRNA fluorescent signal was found in all tested cells when the final HA targeting layer was not included in the particle. These cellular-uptake data indicate that the positively charged sR1P particles were picked up by all cells without selectivity, while the HA coated particles were only uptaken by CD44 expressing cells. CD44 targeted delivery could be achieved using this simple approach.

The specific gene silencing effect was further examined in MDA-MB231 cell (CD44+). To confirm that the gene silencing effect is sequence dependent, a scramble siRNA, which has the same length but randomized sequence, was formulated the same and included in the study as a negative control. Using the above described protocol, a clear gene silencing effect was observed with the HA targeted particle, 60% inhibition (Figure 25). When the specific siRNA was replaced with the scrambled siRNA, the silencing effect was insignificant (<15%). These data reveal that the HA could assist the delivery of siRNA to achieve sequence specific silencing of the luciferase gene.

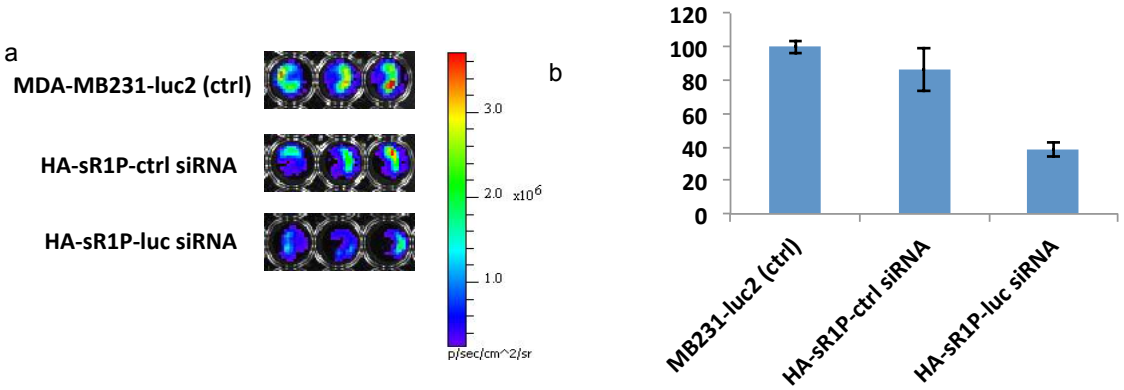

Figure 25. *In vitro* gene-silencing effect of sR1P. The luminescence signal and the luminescence intensity (photons s^{-1}) in MDA-MB231-luc2 cells (a) after incubation for 2h hrs with various particles. The luminescence intensity of untreated cells was set as 100 %. The results are representative of three independent experiments.

KEY RESEARCH ACCOMPLISHMENTS: Bulleted list of key research accomplishments emanating from this research.

- Identified a peptide substrate sequence for SpeB
- Developed a SpeB activatable fluorescent probe for bacterial imaging and detection
- Developed an assembling protocol for ESNM preparation
- Optimized the signal amplification ratio.
- Developed a long-lasting fluorescence imaging probe for cell tracking study.
- Developed a novel bifunctional ESNM to report cell viability.
- Developed an enzyme dependent siRNA delivery system with a persistent gene silencing effect.
- Developed a targeting approach to direct ESNM delivery

REPORTABLE OUTCOMES:

Publication:
Lee SK, Han MS, Tung CH
Layered nanoprobe for long-lasting fluorescent cell label
Small, 2012, 8, 3315-3320.

Lee SK, Tung CH
A fabricated siRNA nanoparticle for ultralong gene silencing in vivo
Adv Funct Mater, 2013, 23, 3488-3493.

Abstract:
A fabricated siRNA nanoparticle capable of ultra-long gene silencing *in vivo.*
Oligonucleotide therapy society, Boston, MA, 10/2012

Presentation:
In vivo molecular imaging. Southern Biomedical Engineering Conference, Houston, TX. 5/2012.

Making tumors glow in the dark – Enzyme responsive probes for tumor imaging. Weill Cornell Brain and Spine Center, New York, NY. 06/2012

Enzyme responsive constructs for imaging and treatment. Roswell Park Cancer Institute, Buffalo, NY. 08/2012

Enzyme responsive nanomedicine for imaging and treatment. Department of Chemistry, Chinese University of Hong Kong, Hong Kong, 10/2012

CONCLUSION:

Recent advances in cell therapies, such as T-cell, islet cell, myocyte, and stem cell therapies, have opened new possibilities in various clinical applications (*3-5*). To further improve their therapeutic value, information about the location, functionality, and fate of injected cells is vital (*6-8*). Conventional techniques, such as histology, do provide clear evidence but require biopsies and thus, cannot provide real-time information. Imaging is the best and only non-invasive way to track injected cells *in vivo*. To follow the injected cells, they were labeled with the developed long-lasting imaging ESNM. The tightly packed polyelectrolytes showed slow intracellularly proteolytic degradation, so that the attached fluorochromes were not released at once, and this slow-release process resulted in a persistent supply of fluorochromes, maintaining the intracellular fluorescence signal at a high level for a prolonged period. Potentially the release kinetics could be controlled by varying polyelectrolytes with different properties, such as length, ionic strength and bond stability. A systemic evaluation of the negatively charged polyelectrolytes is currently under study for a better-controlled probe. Because each particle acts as a reservoir, the developed nanoprobe also worked well with dividing cells. During division, the nanoprobes could be distributed into daughter cells, and then refilled the daughter cells with newly released fluorochromes. When FITC reporter was replaced by an near-infrared reporter, the developed long-lasting labeling strategy could have enormous potential in *in vivo* tracking of cells, because the intracellular fluorescence signal lasts for weeks, much longer than current labeling approaches.

The PLL and PDL containing bifuncational ESNM is also an exciting development. This is the first report that a single ESNM could report two health conditions of cells. After labeling, all healthy cells show one color, but, when the status of the cells is changed from healthy to apoptosis, the dying cells give a second color. This color indicator would be extremely useful in accessing the fate of injected cells.

Short interfering RNAs (siRNAs)-mediated gene regulation in mammalian cells was first discovered about two decades ago and siRNA has since shown immense potential in treating various diseases by silencing abnormally up-regulated genes.(*9-12*) However, delivering the highly charged siRNA to the targeted cells and enabling the specific target gene silencing effect to persist remains challenging.(*13*) Although huge efforts have been invested to develop effective non-viral siRNA delivery systems, including polyplexes, micelleplexes, and exosome nanoparticles,(*14, 15*) various physiological limitations still hinder the successful clinical translation.(*16, 17*) The main drawbacks of gene silencing using synthetic siRNA are transient silencing due to the biodegradation of siRNA, siRNA dilution upon cell division, and its nonrenewable-nature.(*18*) To obtain a consistent silencing effect *in vivo*, it usually requires repetitive administration of the agent.(*19*) However, such repeated injections have resulted in a substantial impediment to patient treatment, as evidenced by decreased enrollment in clinical trials and decreased patient compliance.(*20*) Complete and prolonged gene silencing with a single treatment would offer enormous benefits for chronic diseases, scaling down the administration frequency in dosing schedule.(*21*)

To achieve long-lasting controlled release and gene silencing effects, various groups have developed novel delivery systems for slow and sustained release of the oligonucleotide or siRNA.(*13, 21, 22*) Several trials have also extended into primary T lymphocytes and human stem cells for prolonged gene silencing.(*23, 24*) Although promising cell culture results were obtained in those studies, the actual *in vivo* efficiency remains to be demonstrated. By using the layering deposition technology, we successfully fabricated ESNM by electrostatic interaction, which contain multi-layers of protease degradable PLL and synthetic siRNA. The positively charged ESNM and the targeted ESNM were taken up by cells efficiently, and, once inside the cells, the PLL was gradually degraded by intracellular proteases, resulting in the continuous release of siRNA. These intracellular ESNMs act as siRNA reservoirs, providing siRNA to inhibit their target genes. Upon cell division, the nano-reservoirs were distributed to daughter cells and continued to release siRNA for an extended period of time. Due to extraordinary persistent gene silencing effect, functionalized multilayered ESNM are expected to have great potentials in the areas of cancer therapy, in case luciferase siRNA replaced with siRNA of oncogenes which are predominantly overexpressed in various tumors.

REFERENCES: List all references pertinent to the report using a standard journal format (i.e. format used in Science, Military Medicine, etc.).

(1) Nomizu, M., Pietrzynski, G., Kato, T., Lachance, P., Menard, R., and Ziomek, E. (2001) Substrate specificity of the streptococcal cysteine protease. *J Biol Chem 276*, 44551-6.

(2) Mansouri, S., Winnik, F. M., and Tabrizian, M. (2009) Modulating the release kinetics through the control of the permeability of the layer-by-layer assembly: a review. *Expert Opin Drug Deliv 6*, 585-97.

(3) Sherman, W. (2007) Myocyte replacement therapy: skeletal myoblasts. *Cell transplantation 16*, 971-5.

(4) June, C. H. (2007) Principles of adoptive T cell cancer therapy. *The Journal of clinical investigation 117*, 1204-12.

(5) Cartier, N., Hacein-Bey-Abina, S., Bartholomae, C. C., Veres, G., Schmidt, M., Kutschera, I., Vidaud, M., Abel, U., Dal-Cortivo, L., Caccavelli, L., Mahlaoui, N., Kiermer, V., Mittelstaedt, D., Bellesme, C., Lahlou, N., Lefrere, F., Blanche, S., Audit, M., Payen, E., Leboulch, P., l'Homme, B., Bougneres, P., Von Kalle, C., Fischer, A., Cavazzana-Calvo, M., and Aubourg, P. (2009) Hematopoietic stem cell gene therapy with a lentiviral vector in X-linked adrenoleukodystrophy. *Science (New York, N.Y 326*, 818-23.

(6) Nguyen, P. K., Lan, F., Wang, Y., and Wu, J. C. (2011) Imaging: guiding the clinical translation of cardiac stem cell therapy. *Circulation research 109*, 962-79.

(7) Budde, M. D., and Frank, J. A. (2009) Magnetic tagging of therapeutic cells for MRI. *J Nucl Med 50*, 171-4.

(8) Fujisaki, J., Wu, J., Carlson, A. L., Silberstein, L., Putheti, P., Larocca, R., Gao, W., Saito, T. I., Lo Celso, C., Tsuyuzaki, H., Sato, T., Cote, D., Sykes, M., Strom, T. B., Scadden, D. T., and Lin, C. P. (2011) In vivo imaging of Treg cells providing immune privilege to the haematopoietic stem-cell niche. *Nature 474*, 216-9.

(9) Elbashir, S. M., Harborth, J., Lendeckel, W., Yalcin, A., Weber, K., and Tuschl, T. (2001) Duplexes of 21-nucleotide RNAs mediate RNA interference in cultured mammalian cells. *Nature 411*, 494-8.

(10) Zamore, P. D. (2006) RNA interference: big applause for silencing in Stockholm. *Cell 127*, 1083-6.

(11) Bumcrot, D., Manoharan, M., Koteliansky, V., and Sah, D. W. (2006) RNAi therapeutics: a potential new class of pharmaceutical drugs. *Nature chemical biology 2*, 711-9.

(12) Burnett, J. C., and Rossi, J. J. (2012) RNA-based therapeutics: current progress and future prospects. *Chemistry & biology 19*, 60-71.

(13) Lobovkina, T., Jacobson, G. B., Gonzalez-Gonzalez, E., Hickerson, R. P., Leake, D., Kaspar, R. L., Contag, C. H., and Zare, R. N. (2011) In vivo sustained release of siRNA from solid lipid nanoparticles. *ACS nano 5*, 9977-83.

(14) Gary, D. J., Lee, H., Sharma, R., Lee, J. S., Kim, Y., Cui, Z. Y., Jia, D., Bowman, V. D., Chipman, P. R., Wan, L., Zou, Y., Mao, G., Park, K., Herbert, B. S., Konieczny, S. F., and Won, Y. Y. (2011) Influence of nano-carrier architecture on

in vitro siRNA delivery performance and in vivo biodistribution: polyplexes vs micelleplexes. *ACS nano 5*, 3493-505.

(15) Alvarez-Erviti, L., Seow, Y., Yin, H., Betts, C., Lakhal, S., and Wood, M. J. (2011) Delivery of siRNA to the mouse brain by systemic injection of targeted exosomes. *Nature biotechnology 29*, 341-5.

(16) Schmidt, C. (2011) RNAi momentum fizzles as pharma shifts priorities. *Nature biotechnology 29*, 93-4.

(17) Pecot, C. V., Calin, G. A., Coleman, R. L., Lopez-Berestein, G., and Sood, A. K. (2011) RNA interference in the clinic: challenges and future directions. *Nature reviews 11*, 59-67.

(18) Takabatake, Y., Isaka, Y., Mizui, M., Kawachi, H., Takahara, S., and Imai, E. (2007) Chemically modified siRNA prolonged RNA interference in renal disease. *Biochemical and biophysical research communications 363*, 432-7.

(19) Merritt, W. M., Lin, Y. G., Spannuth, W. A., Fletcher, M. S., Kamat, A. A., Han, L. Y., Landen, C. N., Jennings, N., De Geest, K., Langley, R. R., Villares, G., Sanguino, A., Lutgendorf, S. K., Lopez-Berestein, G., Bar-Eli, M. M., and Sood, A. K. (2008) Effect of interleukin-8 gene silencing with liposome-encapsulated small interfering RNA on ovarian cancer cell growth. *Journal of the National Cancer Institute 100*, 359-72.

(20) Tanaka, T., Mangala, L. S., Vivas-Mejia, P. E., Nieves-Alicea, R., Mann, A. P., Mora, E., Han, H. D., Shahzad, M. M., Liu, X., Bhavane, R., Gu, J., Fakhoury, J. R., Chiappini, C., Lu, C., Matsuo, K., Godin, B., Stone, R. L., Nick, A. M., Lopez-Berestein, G., Sood, A. K., and Ferrari, M. (2010) Sustained small interfering RNA delivery by mesoporous silicon particles. *Cancer research 70*, 3687-96.

(21) Raemdonck, K., Vandenbroucke, R. E., Demeester, J., Sanders, N. N., and De Smedt, S. C. (2008) Maintaining the silence: reflections on long-term RNAi. *Drug discovery today 13*, 917-31.

(22) Bulut, S., Erkal, T. S., Toksoz, S., Tekinay, A. B., Tekinay, T., and Guler, M. O. (2011) Slow release and delivery of antisense oligonucleotide drug by self-assembled peptide amphiphile nanofibers. *Biomacromolecules 12*, 3007-14.

(23) Mantei, A., Rutz, S., Janke, M., Kirchhoff, D., Jung, U., Patzel, V., Vogel, U., Rudel, T., Andreou, I., Weber, M., and Scheffold, A. (2008) siRNA stabilization prolongs gene knockdown in primary T lymphocytes. *European journal of immunology 38*, 2616-25.

(24) Rosner, M., Siegel, N., Fuchs, C., Slabina, N., Dolznig, H., and Hengstschlager, M. (2010) Efficient siRNA-mediated prolonged gene silencing in human amniotic fluid stem cells. *Nature protocols 5*, 1081-95.

APPENDICES: Attach all appendices that contain information that supplements, clarifies or supports the text. Examples include original copies of journal articles, reprints of manuscripts and abstracts, a curriculum vitae, patent applications, study questionnaires, and surveys, etc.

Appendix 1:
Lee SK, Han MS, Tung CH
Layered nanoprobe for long-lasting fluorescent cell label
Small, 2012, 8, 3315-3320.

Appendix 2:
Lee SK, Tung CH
A fabricated siRNA nanoparticle for ultralong gene silencing in vivo
Adv Funct Mater, 2013, 23, 3488-3493.

small NANO MICRO

Fluorescent Probes

Layered Nanoprobe for Long-Lasting Fluorescent Cell Label

*Seung Koo Lee, Myung Shin Han, and Ching-Hsuan Tung**

***A** long-lasting particle-based fluorescent label is designed for extended cell imaging studies. This onion-like nanoprobe is constructed through layer-by-layer fabrication technology. The nanoprobes are assembled with multiple layers of optically quenched polyelectrolytes, the fluorescence signal of which can be released later by intracellular proteolysis. Upon incubation with cells, the assembled nanoprobes are taken up efficiently. The tight packing and layered assembly of the quenched polyelectrolytes slow subsequent intracellular degradation, and then result in a prolonged intracellular fluorescence signal for up to 3 weeks with no noticeable toxicity.*

1. Introduction

Layer-by-layer fabrication technology has been used to develop biomaterials for various biological applications.[1–5] One major advantage of this fabrication technology is that materials with different properties could be layered sequentially, thereby resulting in a multifunctional assembly. Recent advances in cell therapies, such as T-cell, islet cell, myocyte, and stem cell therapies, have opened new possibilities in various clinical applications.[6–9] To further improve their therapeutic value, information about the location, functionality, and fate of injected cells is vital.[10–12] Monitoring cell trafficking inside the body is important, and conventional techniques, such as histology, do provide clear evidence but require biopsies, and thus cannot provide real-time information.

Imaging is the best and only noninvasive way to track injected cells in vivo. To follow injected cells, they must be labeled with appropriate imaging reporters that offer bright signals for extended periods of time with no cytotoxicity. Ineffective labeling approaches would reduce the sensitivity and limit the duration of studies. Several transgenic reporters, such as green fluorescent protein, luciferase, and thymidine kinase, can satisfy these prerequisites; however, introducing a foreign gene into therapeutic cells is a concern in clinical applications.[13–15] Chemical reporters, including organic fluorochromes and inorganic nanocrystals, have been used,[16,17] but most chemical reporters provide only transient signals, especially in dividing cells. Recently, we found that multilayered small interfering RNA (siRNA)-coated gold nanoparticles (AuNPs) show extended gene silencing effects in various tumor cells.[5] Based on this observation, we designed a long-lasting imaging nanoprobe for live cell labeling.

Dr. S. K. Lee, M. S. Han, Prof. C.-H. Tung
Department of Translational Imaging
The Methodist Hospital Research Institute
Weill Cornell Medical College
Houston, TX 77030, USA
E-mail: ctung@tmhs.org

DOI: 10.1002/smll.201200751

2. Results and Discussion

A labeling nanoprobe was prepared with multiple layers of polyelectrolytes, sequentially assembled on an inert AuNP, by using alternating charged polymers (**Figure 1**a). AuNPs were selected as the core of the multilayered fluorescent nanoprobe for their uniform size, shape-dependent optical and electronic features, as well as feasibility for surface modification.[18,19] The negatively charged polyelectrolyte used was poly(acrylic acid) (PAA), and the positively charged layer was biodegradable poly-L-lysine (PLL) decorated with fluorescein isothiocyanate (FITC).[20,21] Because the positively charged lysine residues in PLL can be degraded by many intracellular proteases, such as cathepsins B and L, PLL was selected as the backbone to provide a slow-release capability.[22–24] When multiple FITC residues were loaded onto one PLL backbone, self-quenching occurred due to the close proximity of neighboring fluorochromes. Importantly though, this quenched signal could be recovered after proteolytic degradation of the PLL backbone. The optimal loading ratio (FITC/PLL = 10/1) that provided the maximum quenching/dequenching effect and protease accessibility was determined from a series of

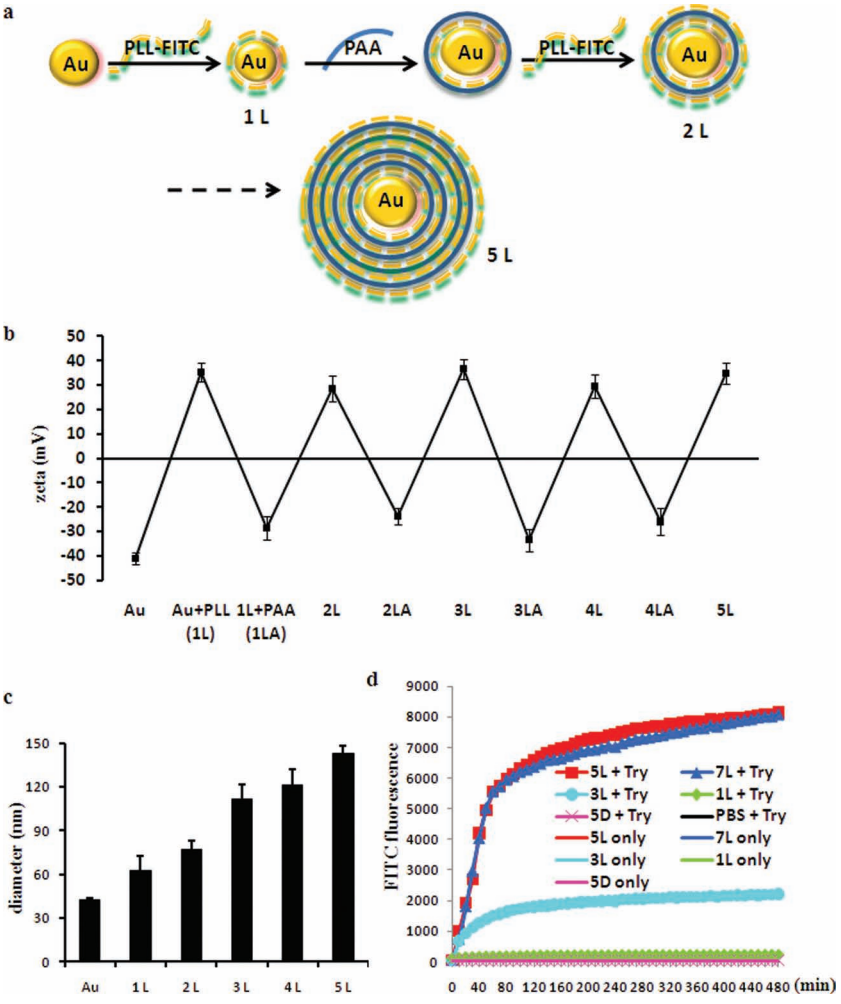

Figure 1. Preparation and characterization of multilayered fluorescent AuNPs. a) Preparation process of multilayered fluorescent AuNPs using PLL-FITC and PAA as the charged polyelectrolytes. b) Zeta potential after each coating of polyelectrolytes. c) Diameter of bare AuNPs and polyelectrolyte-coated AuNPs. d) Protease-assisted FITC release from various AuNPs. Multilayered fluorescent AuNPs (1L: FITC 4.5 nmol, 3L: FITC 6.5 nmol, 5L: FITC 8.5 nmol, 7L: FITC 10.5 nmol, 5D: FITC 11 nmol) were incubated with or without trypsin (Try) in PBS and the fluorescence intensity was examined for up to 8 h.

PLL conjugates with differing amounts of FITC. A greater than 34-fold change in fluorescence signal was observed upon treatment with a model protease, trypsin (Figure S1a, Supporting Information). Higher loading of FITC provided no further benefit. For comparison, FITC was also loaded on a nondegradable poly-D-lysine (PDL) at the same ratio (FITC/PDL = 10/1) and treated in the same way. As expected, the fluorescence signal was not increased (Figure S1b), which suggests that proteolysis is required to release the quenched fluorescence signal.

To assemble the multilayered fluorescent AuNPs, the negatively charged AuNPs (40 nm) in water were dropped into the positively charged PLL-FITC solution (average M_w = 50 kDa) for the first layer of coating. The reaction mixture was incubated for 30 min, and then the coated particles were spun down by centrifugation. After three washes with sterilized water, the PLL-FITC-coated AuNPs (1L AuNPs) were added to the negatively charged PAA (M_w = 15 kDa) solution. By repeating these procedures (Figure 1a), multilayered AuNPs—up to five layers of PLL-FITC and four layers of PAA (5L AuNPs)—were successfully fabricated by electrostatic interactions. The alternating layers of charged polyelectrolytes were evidenced by the zigzag pattern of the surface zeta potentials (Figure 1b). The PLL coating brought the surface charge from negative to positive, whereas the PAA coating switched it from positive to negative. The hydrodynamic diameter of the prepared AuNPs was measured by dynamic light scattering (DLS) after coating with each layer. The size of the initial bare AuNPs was 40 nm and the prepared particle size increased steadily with the number of layers (1L: 63 nm; 3L: 112 nm; 5L: 144 nm; Figure 1c).

AuNPs prepared with different numbers of layers were then subjected to protease activation. As shown in Figure 1d, particles were stable in phosphate-buffered saline (PBS), but when treated with protease the fluorescence signal change was layer-dependent. The optimal formulation was 5L AuNPs (five layers of PLL and four layers of PAA), the fluorescence of which changed by 195-fold. The fluorescence signal change of 7L AuNPs, however, was similar to that of 5L AuNPs despite the two additional layers of PLL-FITC added to the particles. Under the same conditions, when protease-resistant PDL-FITC was used in the assembly, no fluorescence change was seen with the PDL-FITC-coated AuNPs (5D AuNPs, five layers of PDL and four layers of PAA), as observed with the free PDL-FITC peptide (Figure S1b), again suggesting that protease degradation is required to release the packed fluorochromes. Comparing the protease-induced fluorescence changes between free PLL-FITC and assembled particles, a much larger change was seen with the assembled particles. This was presumably caused by the layer-by-layer packing, because fluorescence quenching could occur not only within each PLL molecule but also between layers, and the plasmonic resonance of the Au core.[25,26] Additionally, the kinetics of the fluorescence release of the nanoprobes was much slower than that of free PLL-FITC molecules, which suggests that the protease required more time to digest the tightly packed layers.

The ability of the multilayered fluorescent nanoprobe to label live cells was investigated by comparing the nanoprobe with commercially available cell labeling reagents, CM-DiI and CMTMR, using fluorescence microscopy. HeLa cells were incubated with cell trackers and various multilayered fluorescent nanoprobes (**Figure 2**). When incubated with CMTMR, the fluorescence signal was strong at short time points but

NANO MICRO small

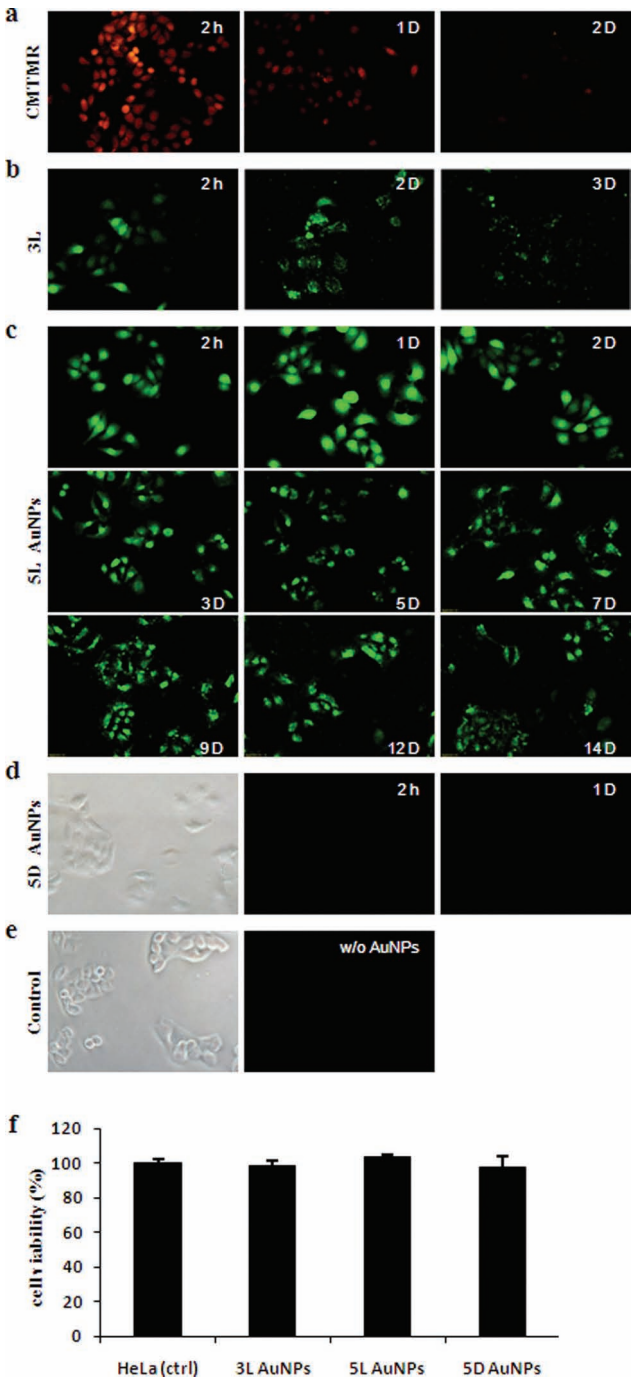

Figure 2. Live cell imaging and cytotoxicity in HeLa cells. After incubation for 30 min with cell tracker CMTMR (a) or incubation for 12 h with various multilayered fluorescent AuNPs, such as 3L (FITC 2.1 nmol) (b), 5L (FITC 2.7 nmol) (c), 5D (FITC 3.6 nmol) (d), and non-treated control (e), fluorescence signals were assessed by fluorescence microscopy (magnification:20×). Cell viability (f) was evaluated after incubation for 24 h with various multilayered fluorescent AuNPs using CellTiter solution.

decreased quickly and lasted only for 2 days (Figure 2a). When incubated with 3L AuNPs, the intracellular fluorescence signal was sustained for approximately 3 days (Figure 2b). However, a prolonged fluorescence signal was found with 5L AuNPs. A high fluorescence signal was maintained for more than 14 days with negligible background (Figure 2c). CM-DiI, PLL-FITC without AuNPs, and 1L AuNPs were also tested with HeLa cells; however, their signal strengths were much weaker than that of the 5L AuNPs (Figure S2). As expected, there was no signal when nondegradable 5D AuNPs were used (Figure 2d).

To investigate the sublocalization of multilayered nanoprobes, HeLa cells were stained with Hoechst 33342 and LysoTracker after treatment with 5L AuNPs (**Figure 3**). Merged fluorescence signals of FITC and LysoTracker clearly showed the lysosomal delivery of multilayered fluorescent nanoprobes. Two hours after incubation, the merged image of FITC and LysoTracker signals in some cells showed significant overlapping, thus indicating the particles were located and activated in lysosomes, whereas in other cells, the FITC fluorescence signal was distributed evenly in whole cells. This suggested that somehow the nanoprobes could flee the lysosomes. At day 3, a high FITC signal was found in the nucleus, which further supported the hypothesis that the particles were able to escape from lysosomes and continue to release fluorescence signals.

Similar signal patterns were seen with MDA-MB231 cells using either commercially available cell trackers or our multilayered fluorescent nanoprobes (Figure S3). However, in MDA-MB231 cells, the fluorescence signal could only be followed for 5 days, because of the fast-growing nature of MDA-MB 231 cells. Among the probes tested, only 5L AuNPs could maintain a strong fluorescence signal to day 5 in MDA-MB231 cells. The cytotoxicity of the prepared multilayered fluorescent nanoprobes was evaluated in HeLa (Figure 2f) and MDA-MB231 (Figure S3g) cells. No significant toxicity was detected in any nanoprobe-treated cells.

To gain a better understanding of signal retention after cell division, a suspension of the Jurkat T-cell line was tested with 5L AuNPs (**Figure 4**a) or the commercially available cell tracking agents, CM-DiI and CMTMR (Figure 4b,c). After incubation with various labels, aliquots of cells were collected and analyzed by flow cytometry (Figure S4). The initial fluorescence intensity of each label was controlled to a similar level for a fair comparison. Similar retention patterns were seen with the CM-DiI and CMTMR cell trackers. The intensity in CM-DiI- and CMTMR-treated cells had declined to 8 and 3% of the original intensity, respectively, after 4 days of incubation. At day 7, the labels were largely gone, and the signal had declined to a background level. As the doubling time of the Jurkat T-cell line is approximately 48 h, this result suggested that the label lasted for about three divisions. In contrast, the 5L AuNPs offered a much longer signal duration. At day 4, the signal intensity was still 24%. At days 7 and 14, the signal had declined to 12 and 7%, respectively. Even after 21 days, the 4% remaining signal was still detectable by fluorescence-activated cell sorting (FACS). These results suggest that the slow release mechanism prolonged the duration of action of the cell labels and that the nanoparticles were suitable for labeling dividing cells.

The potential toxicity of the nanoprobes in Jurkat cells was further assessed by monitoring a T-cell-specific surface marker. Specifically, after treatment with 5L AuNPs, cells were stained with an anti-CD3-phycoerythrin (PE)

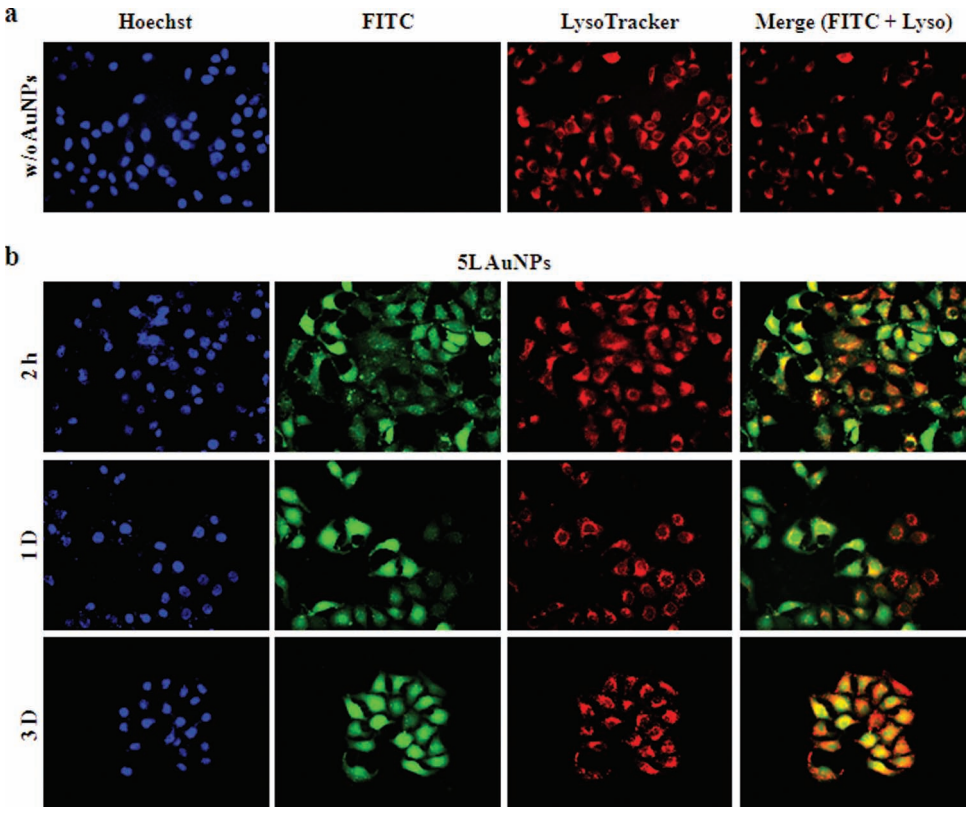

Figure 3. Subcellular localization of the multilayered nanoprobes. HeLa cells were incubated without (a) or with (b) 5L AuNPs (FITC 2.7 nmol) for 12 h and washed three times with PBS. At each time point (2 h, 1 day, and 3 days), cells were stained with LysoTracker (1 μM) for 1 h, Hoechst 33342 (1 μM) for 5 min and then the fluorescence signal was investigated by fluorescence microscopy (magnification:40×) using different filter sets (Hoechst 33342:blue; 5L AuNPs:green;LysoTracker: red).

antibody and SYTOX Blue to confirm cell phenotypic integrity and viability, respectively. No significant difference between 5L AuNPs-treated and nontreated cells was seen up to 7 days (**Figure 5**). Near identical FACS scatter plots of the 5L AuNPs-treated and nontreated cells also supported the finding that 5L AuNPs caused no cell damage 21 days after treatment (Figure S51, thereby indicating the safety of this long-lasting nanoprobe.

3. Conclusion

In summary, the tightly packed polyelectrolytes showed slow proteolytic degradation, so that the attached fluorochromes were not released at once, and this slow-release process resulted in a persistent supply of fluorochromes, which maintained the intracellular fluorescence signal at a high level for a prolonged period. Potentially the release kinetics could be controlled by varying polyelectrolytes with different properties, such as length, ionic strength, and bond stability. A systemic evaluation of the negatively charged polyelectrolytes is currently under way for a better-controlled probe. Because each particle acts as a reservoir, the developed nanoprobe also worked well with dividing cells. During division, the nanoprobes could be distributed into daughter cells, and then the daughter cells were

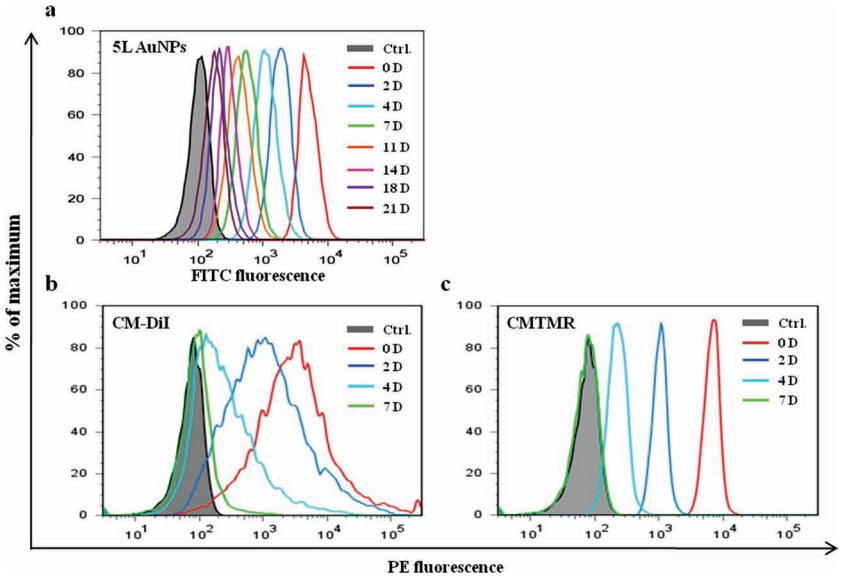

Figure 4. Fluorescence retention through generations in Jurkat cells. After treatment with 5L AuNPs (FITC 13.6 nmol), CM-DiI (1 μM), or CMTMR (2 μM), fluorescence intensity was evaluated by flow cytometry (a–c) for 21 days.

NANO MICRO small

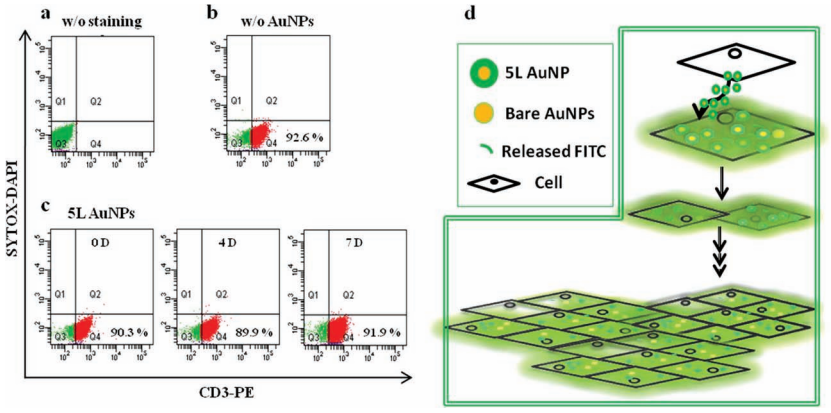

Figure 5. a–c) Cell phenotype and viability after treatment with 5L AuNPs in Jurkat cells. CD3 expression (PE) and cell viability (4′,6-diamidino-2-phenylindole, DAPI) without staining (a) and double staining without treatment (b) or treatment with 5L AuNPs (c) were assessed for 7 days using flow cytometry. d) Illustration of cellular uptake and signal release from multilayered fluorescent AuNPs through generations.

refilled with newly released fluorochromes (Figure 5d). When FITC reporter was replaced by a near-infrared reporter, the developed long-lasting labeling strategy could have enormous potential in *in vivo* tracking of cells, because the intracellular fluorescence signal lasts for weeks, much longer than current labeling approaches.

4. Experimental Section

Chemicals and Materials: Poly-L-lysine (PLL, M_w = 30 000–70 000), poly-D-lysine (PDL, M_w = 30 000–70 000), poly(acrylic acid) (PAA, 35 wt% solution, average M_w = 15 000), fluorescein 5(6)-isothiocyanate (FITC), and the monoclonal anti-CD3-PE antibody were obtained from Sigma–Aldrich (St. Louis, MO). Bare AuNPs (40 nm) were purchased from BB International (Cardiff, UK). SYTOX Blue, CM-DiI, CMTMR, Hoechst 33342, and LysoTracker were from Invitrogen (Carlsbad, CA). Amicon Ultracel membranes (10 kDa) were from Millipore (Billerica, MA), and CellTiter aqueous one solution was from Promega (Madison, WI).

Preparation of PLL-FITC and PDL-FITC: Different amounts of FITC (0.1, 0.2, 0.4, 0.6, 0.8, or 1.0 mg) in dimethylformamide (DMF) solution (500 μL) were reacted with PLL or PDL (1 mg) in $NaHCO_3$ (1 mM, 500 μL) with constant shaking in the dark at room temperature for 2 h. The reaction products were separated using molecular-weight-cutoff membrane filters (10 kDa, Millipore). The resulting PLL-FITC and PDL-FITC were collected and washed several times with sterilized water until the color was clear.

Proteolytic Activation of PLL-FITC: To measure the dequenching effect, the prepared PLL-FITC (PLL 0.2 nmol in 5 μL) and PDL-FITC (PDL 0.2 nmol in 5 μL) in PBS were incubated with trypsin–ethylenediamine tetraacetic acid (EDTA; 10 μL, 0.25%, Sigma–Aldrich) in a 96-well culture plate at 37 °C, and the increase in the FITC fluorescence signal was assessed using a Spectramax M2 plate reader (Molecular Devices, Sunnyvale, CA) at 480 nm excitation and 530 nm emission for 3 h.

Preparation of Multilayered Fluorescent AuNPs: AuNP solution (40 nm, 3.15×10^9 particles in 700 μL) was added dropwise to a PLL-FITC solution (PLL, 1.8 nmol in 500 μL). After incubating for 30 min in the dark with gentle shaking, the solution was centrifuged (30 min at 16 100 *g*) using a microcentrifuge (Eppendorf, Hauppauge, NY). The supernatant was removed, and the gel-like deep red pellet was suspended in pure water and centrifuged again (30 min at 16 100 *g*). After a further wash, PLL-FITC-coated AuNPs were resuspended in pure water (500 μL). Next, the PLL-FITC-coated AuNPs were added to a PAA solution (23.3 mM, 500 μL). The reaction solution was incubated in the dark for 30 min with gentle shaking, followed by three washes. The deposition procedures were repeated for a total of nine layers of polyelectrolyte (five layers of PLL-FITC and four layers of PAA). Zeta potentials of prepared AuNPs in water were measured using a Zeta-PALS apparatus (Brookhaven, Holtsville, NY) and sizes were measured using a Zetasizer Nano-ZS instrument (Malvern, Worcestershire, UK) according to the manufacturer's protocol.

Protease-Assisted Fluorescence Release from Multilayered AuNPs: The protease-induced fluorescence change of the multilayered fluorescent AuNPs was determined by incubating various formulated particles (7.88×10^8 particles) in a 96-well culture plate with or without trypsin (25 μL) in PBS at 37 °C. The increase in the FITC fluorescence signal was analyzed using a Spectramax M2 plate reader (Molecular Devices) at 480 nm excitation and 530 nm emission for 8 h.

Cell Lines: HeLa cells and MDA-MB231 human breast cancer cells were cultured in Dulbecco's modified Eagle's medium (DMEM; Mediatech Inc., Manassas, VA), and Jurkat cells were cultured in RPMI 1640 medium (Thermo Scientific, Rockford, IL). All culture media were supplemented with 2 mM L-glutamine, 100 U mL^{-1} penicillin, 100 mg mL^{-1} streptomycin, and 10% heat-inactivated fetal bovine serum (Sigma–Aldrich) in a humidified atmosphere with 5% CO_2 at 37 °C.

Live Cell Imaging Using Fluorescence Microscopy: Fluorescence images of live cells were acquired using a fluorescence microscopy system (Olympus, Tokyo, Japan). Briefly, HeLa and MDA-MB231 cells were collected by trypsinization, counted, and plated in a 96-well black clear-bottom culture plate (Corning Life Sciences, Pittston, PA) at a density of 1×10^3 cells per well. After 1 day, AuNPs (2.52×10^8 particles) were added and incubated for 12 h. Cells were then washed three times with PBS, cultured in phenol red-free medium, and imaged with a fluorescence microscope at the time points indicated. In a separate set of experiments, cells were treated with cell trackers CM-DiI (2 μM) or CMTMR (7.5 μM, Invitrogen). One day after cell seeding, HeLa and MDA-MB231 cells were incubated with CM-DiI for 5 min at 37 °C and then further incubated at 4 °C for an additional 15 min according to the manufacturer's protocol. For CMTMR studies, cells were incubated with CMTMR for 30 min at 37 °C, the medium was replaced with fresh medium, and incubation was performed for a further 30 min. After labeling with CM-DiI or CMTMR, cells were washed three times with PBS, cultured in phenol red-free medium, and imaged under a fluorescence microscope as indicated.

For the sublocalization of multilayered nanoprobes, HeLa cells were collected by trypsinization, counted, and plated in a 96-well

black clear-bottom culture plate (Corning Life) at a density of 1×10^3 cells per well. After 1 day, AuNPs (2.52×10^8 particles) were added and incubated for 12 h. Cells were then washed three times with PBS and cultured in phenol red-free medium. At each time point (2 h, 1 day, and 3 day), cells were stained with LysoTracker (1 μM, Invitrogen) for 1 h and Hoechst 33342 (1 μM, Invitrogen) for 5 min at 37 °C according to the manufacturer's protocol. After three washes with PBS, cells were imaged under a fluorescence microscope.

Cytotoxicity Assessment of the Multilayered Fluorescent AuNPs: A cell proliferation assay was performed to assess the cytotoxicity of the various treatments. Briefly, HeLa and MDA-MB231 cells were collected by trypsinization, counted, and plated in a 96-well culture plate at a density of 5×10^3 cells per well. One day after seeding, AuNPs (2.52×10^8 particles) were added and the cells were cultured for a further 24 h. At day 2, CellTiter solution (20 μL, Promega) was added to each well, incubation was performed for an additional 3 h, and then the absorbance of the solution was measured at 490 nm using a Spectramax M2 plate reader (Molecular Devices).

Fluorescence Retention in Jurkat Cells: Jurkat cells (1.0×10^6 cells) were seeded in a 12-well culture plate (BD Falcon, San Jose, CA) together with 5L AuNPs (1.26×10^9 particles) in RPMI 1640 medium (400 μL) and cultured for 24 h in the dark at 37 °C in a 5% CO_2 atmosphere. Cells (4×10^5) were then transferred to a FACS tube after three washes with PBS, and the FITC fluorescence signal inside the cells was measured using a BD LSR II flow cytometer (BD Biosciences, San Jose, CA). The remaining cells were cultured in six-well culture plates (BD Falcon) in RPMI 1640 medium (4 mL). The procedure was repeated at different time points, up to 21 days. In a separate set of experiments, Jurkat cells (1.0×10^6) were incubated with CM-DiI (1 μM) or CMTMR (2 μM) following the manufacturer's instructions. On the designated day, the fluorescence signal of CM-DiI or CMTMR was measured using a PE filter set by a BD LSR II flow cytometer.

Assessment of CD3 Expression Profiles and Cytotoxicity after Treatment with 5L AuNPs: One day after incubating Jurkat cells (1.0×10^6) with 5L AuNPs (1.26×10^9 particles) in a 12-well culture plate in RPMI medium (400 μL), a fraction of the cells (4×10^5) was moved to a FACS tube, followed by three PBS washes. Anti-CD3 antibody (3 μL, Sigma–Aldrich) and SYTOX Blue (2 μL, Invitrogen) in PBS (1 mL) were added according to the manufacturer's instructions. PE fluorescence for CD3 expression and DAPI for cytotoxicity in Jurkat cells were measured for up to 7 days using a BD LSR II flow cytometer.

Supporting Information

Supporting Information is available from the Wiley Online Library or from the author.

Acknowledgements

This research was supported in part by NIH CA135312, DOD W81XWH-10-1-0597, DOD W81XWH-11-1-0442, and the Golfers Against Cancer Foundation.

[1] C. S. Peyratout, L. Dahne, *Angew. Chem. Int. Ed.* **2004**, *43*, 3762.
[2] C. M. Jewell, D. M. Lynn, *Adv. DrugDelivery Rev.* **2008**, *60*, 979.
[3] H. Ai, S. A. Jones, Y. M. Lvov, *Cell Biochem. Biophys.* **2003**, *39*, 23.
[4] N. Reum, C. Fink-Straube, T. Klein, R. W. Hartmann, C. M. Lehr, M. Schneider, *Langmuir* **2010**, *26*, 16901.
[5] S. K. Lee, M. S. Han, S. Asokan, C. H. Tung, *Small* **2011**, *7*, 364.
[6] C. H. June, *J. Clin. Invest.* **2007**, *117*, 1204.
[7] P. A. Halban, M. S. German, S. E. Kahn, G. C. Weir, *J. Clin. Endocrinol. Metab.* **2010**, *95*, 1034.
[8] W. Sherman, *Cell Transplant.* **2007**, *16*, 971.
[9] N. Cartier, S. Hacein-Bey-Abina, C. C. Bartholomae, G. Veres, M. Schmidt, I. Kutschera, M. Vidaud, U. Abel, L. Dal-Cortivo, L. Caccavelli, N. Mahlaoui, V. Kiermer, D. Mittelstaedt, C. Bellesme, N. Lahlou, F. Lefrere, S. Blanche, M. Audit, E. Payen, P. Leboulch, B. l'Homme, P. Bougneres, C. Von Kalle, A. Fischer, M. Cavazzana-Calvo, P. Aubourg, *Science* **2009**, *326*, 818.
[10] J. Fujisaki, J. Wu, A. L. Carlson, L. Silberstein, P. Putheti, R. Larocca, W. Gao, T. I. Saito, C. Lo Celso, H. Tsuyuzaki, T. Sato, D. Cote, M. Sykes, T. B. Strom, D. T. Scadden, C. P. Lin, *Nature* **2011**, *474*, 216.
[11] P. K. Nguyen, F. Lan, Y. Wang, J. C. Wu, *Circ. Res.* **2011**, *109*, 962.
[12] M. D. Budde, J. A. Frank, *J. Nucl. Med.* **2009**, *50*, 171.
[13] M. Rodriguez-Porcel, *Curr. Cardiol. Rep.* **2010**, *12*, 51.
[14] S. Hacein-Bey-Abina, C. Von Kalle, M. Schmidt, M. P. McCormack, N. Wulffraat, P. Leboulch, A. Lim, C. S. Osborne, R. Pawliuk, E. Morillon, R. Sorensen, A. Forster, P. Fraser, J. I. Cohen, G. de Saint Basile, I. Alexander, U. Wintergerst, T. Frebourg, A. Aurias, D. Stoppa-Lyonnet, S. Romana, I. Radford-Weiss, F. Gross, F. Valensi, E. Delabesse, E. Macintyre, F. Sigaux, J. Soulier, L. E. Leiva, M. Wissler, C. Prinz, T. H. Rabbitts, F. Le Deist, A. Fischer, M. Cavazzana-Calvo, *Science* **2003**, *302*, 415.
[15] X. Guo, L. Huang, *Acc. Chem. Res.* **2012**, 45, 971.
[16] A. Boissonnas, L. Fetler, I. S. Zeelenberg, S. Hugues, S. Amigorena, *J. Exp. Med.* **2007**, *204*, 345.
[17] U. Resch-Genger, M. Grabolle, S. Cavaliere-Jaricot, R. Nitschke, T. Nann, *Nat. Methods* **2008**, *5*, 763.
[18] M. C. Daniel, D. Astruc, *Chem. Rev.* **2004**, *104*, 293.
[19] J. H. Lee, K. Lee, S. H. Moon, Y. Lee, T. G. Park, J. Cheon, *Angew. Chem. Int. Ed.* **2009**, *48*, 4174.
[20] H. Jans, K. Jans, L. Lagae, G. Borghs, G. Maes, Q. Huo, *Nanotechnology* **2010**, *21*, 455702.
[21] K. Kim, J. W. Lee, J. Y. Choi, K. S. Shin, *Langmuir* **2010**, *26*, 19163.
[22] R. Weissleder, C. H. Tung, U. Mahmood, A. Bogdanov, Jr., *Nat. Biotechnol.* **1999**, *17*, 375.
[23] M. Funovics, R. Weissleder, C. H. Tung, *Anal. Bioanal. Chem.* **2003**, *377*, 956.
[24] Y. Choi, R. Weissleder, C. H. Tung, *Cancer Res.* **2006**, *66*, 7225.
[25] K. Kim, B. H. Sohn, J. I. Jin, *J. Nanosci. Nanotechnol.* **2005**, *5*, 1898.
[26] T. Mangeat, A. Berthier, C. Elie-Caille, M. Perrin, W. Boireau, C. Pieralli, B. Wacogne, *Laser Phys.* **2009**, *2*, 252.

Received: April 6, 2012
Revised: May 15, 2012
Published online: August 7, 2012

Submitted to small NANO MICRO

Supporting Information

Layered nanoprobe for long-lasting fluorescent cell label

Seung Koo Lee, Myung Shin Han, and Ching-Hsuan Tung*

Department of Translational Imaging, The Methodist Hospital Research Institute, Weill Cornell Medical College, Houston, Texas 77030, USA.

*e-mail: ctung@tmhs.org

Figure S1. Protease-assisted cleavage of PLL or PDL conjugated with FITC. After incubation of different concentration of PLL-FITC (a) or PDL-FITC (b) with or without trypsin in PBS, the fluorescence intensity was examined until 3 h.

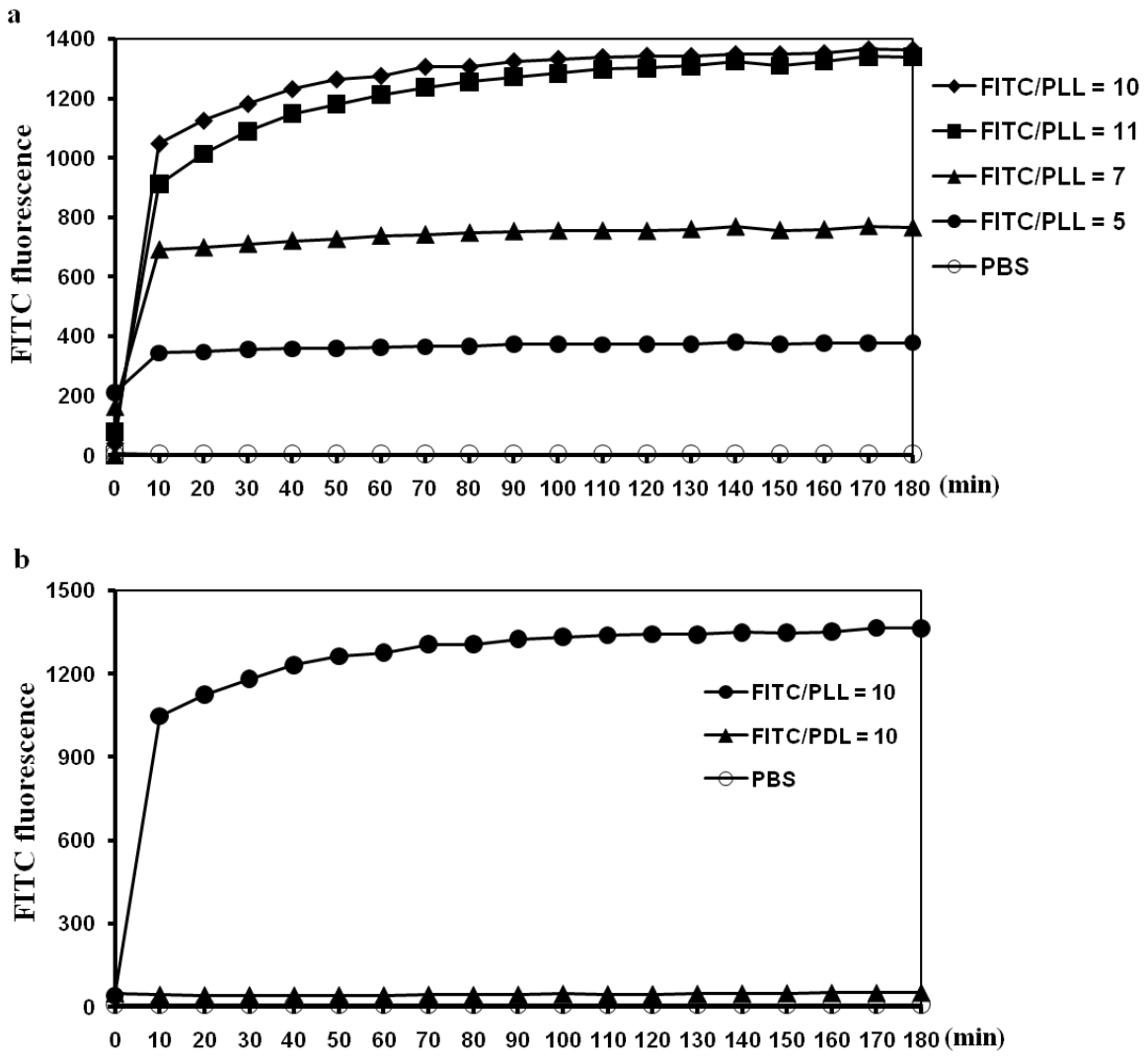

Figure S2. Live cell imaging in HeLa cells with time course . After incubation with CM-DiI, 2 μM (a) for 30 min, PLL-FITC (b) for 4 h, or 1L AuNPs (FITC 1.4 nmole) (c) for 12 h, fluorescence signal was investigated with fluorescence microscopy (magnification : 20 X) in HeLa cells.

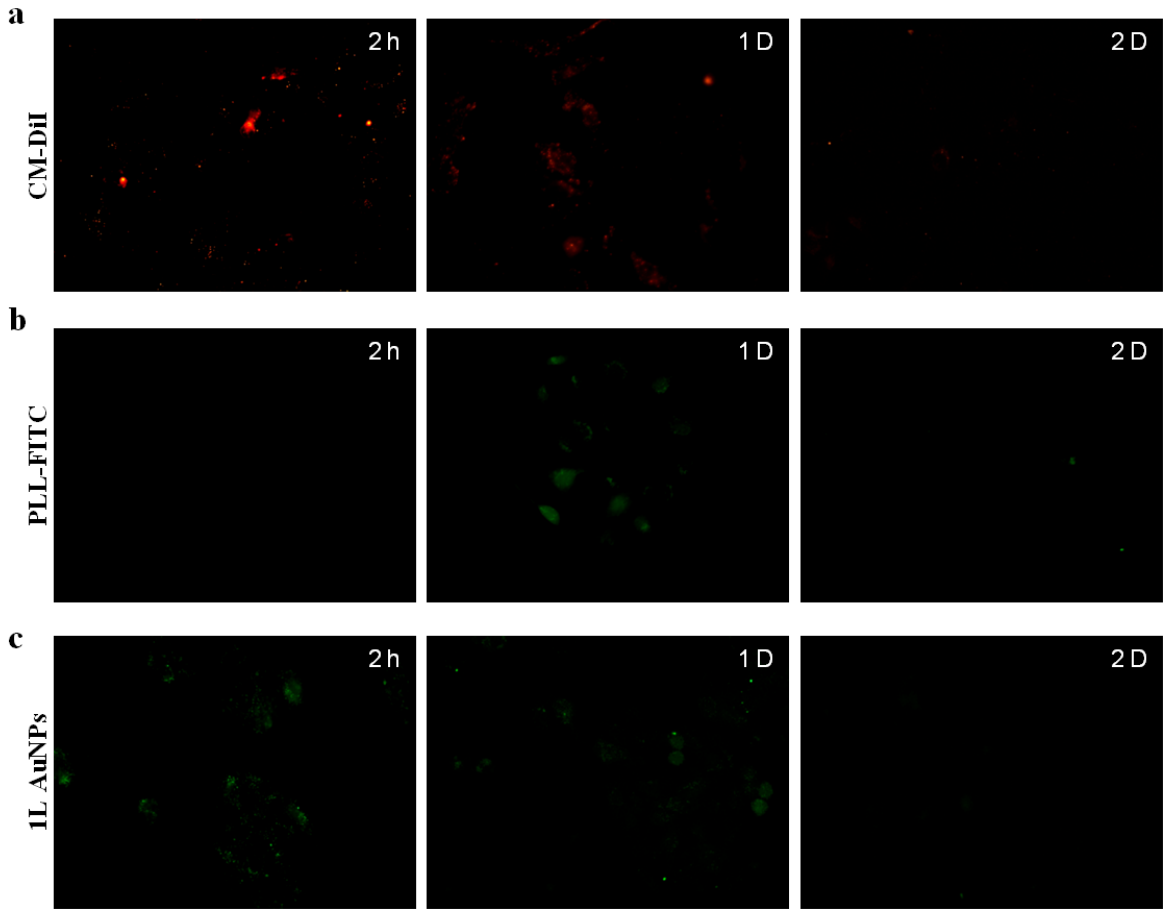

Figure S3. Live cell imaging and cytotoxicity in MDA-MB231 cells. After incubation with cell tracker, CMTMR, 7.5 μM (a) for 15 min, CM-DiI, 2 μM (b) for 30 min, or various multilayered fluorescent AuNPs, such as 3L (FITC 2.1 nmole) (c), 5L (FITC 2.7 nmole) (d) and 5D (FITC 3.6 nmole) (f) for 12 h, fluorescence signal was investigated with fluorescence microscopy (magnification : 20 X). Cell viability (g) was also evaluated after incubation for 24 h with various multilayered fluorescent AuNPs using CellTiter solution in MDA-MB231 cells.

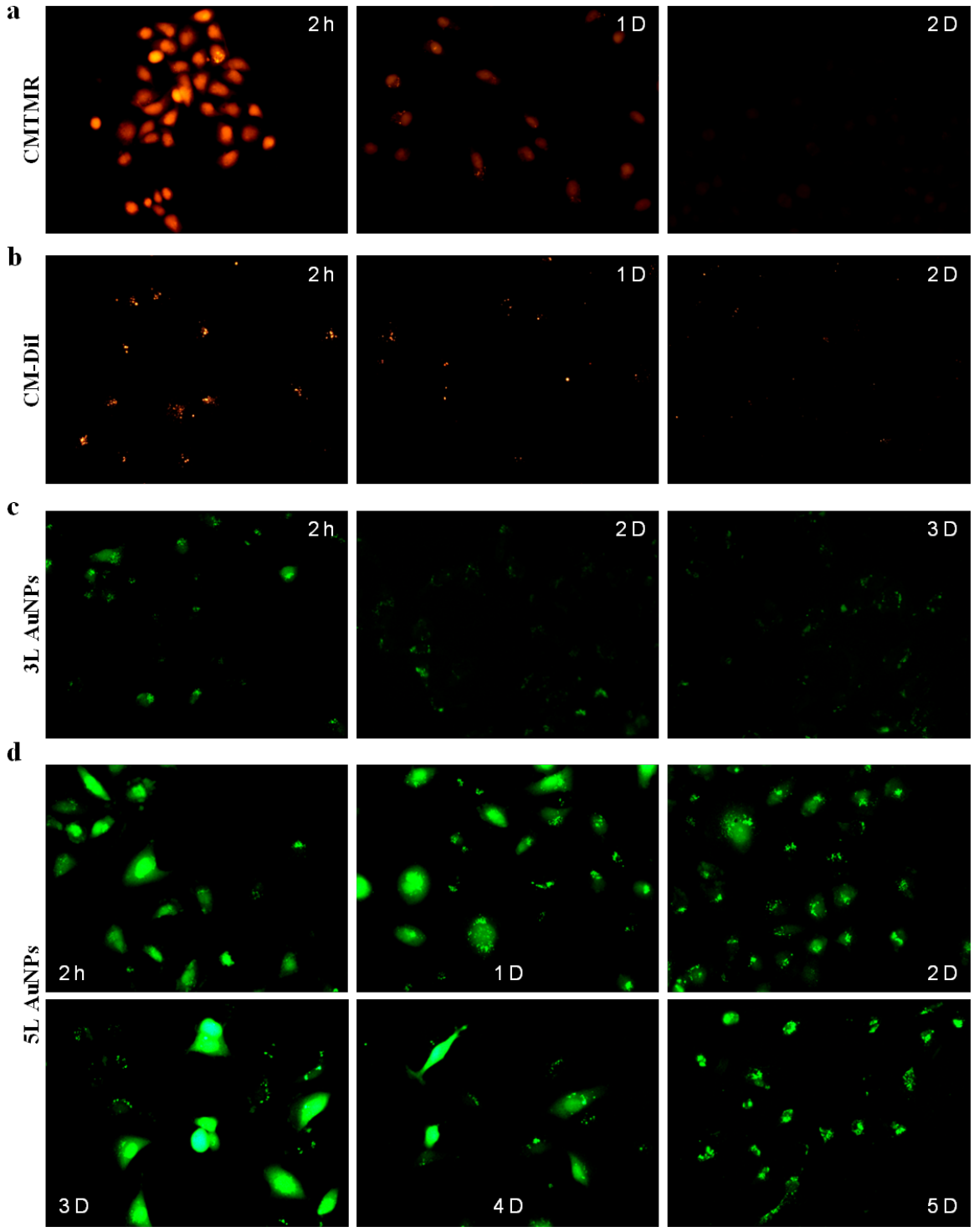

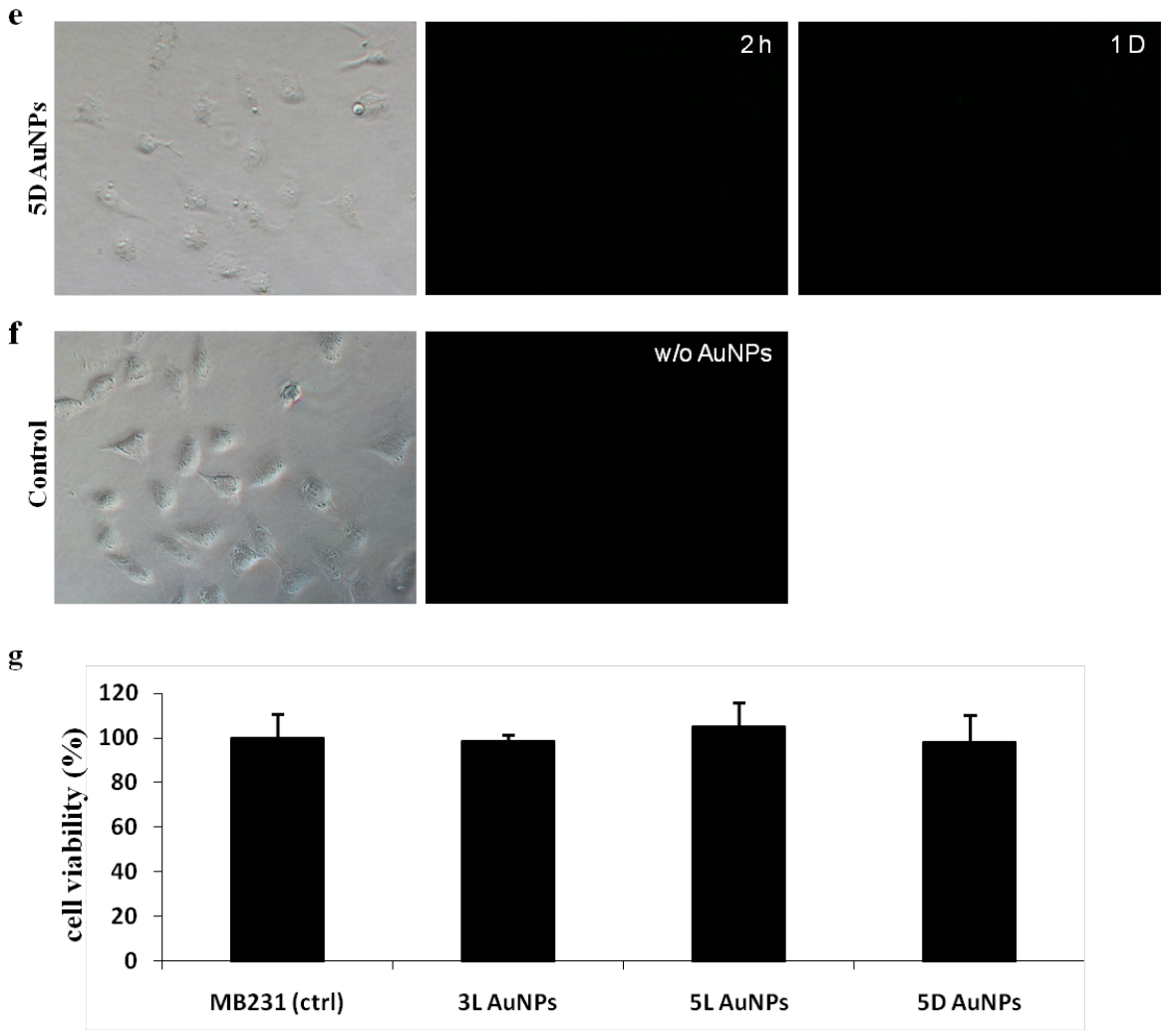
e
5D AuNPs
2 h
1 D
f
Control
w/o AuNPs
g
cell viability (%)
120
100
80
60
40
20
0
MB231 (ctrl)
3L AuNPs
5L AuNPs
5D AuNPs

Figure S4. Cell population and fluorescence intensity of Jurkat cells. After treatment with 5L AuNPs (FITC 13.6 nmole) (a), CM-DiI, 1 μM (b) or CMTMR, 2 μM (c) to Jurkat cells, fluorescence intensity was measured by flow cytometry with time course. Inserted number in each column shows the average fluorescence intensity value and the percentage, the intensity at 0 Day was set as 100 %.

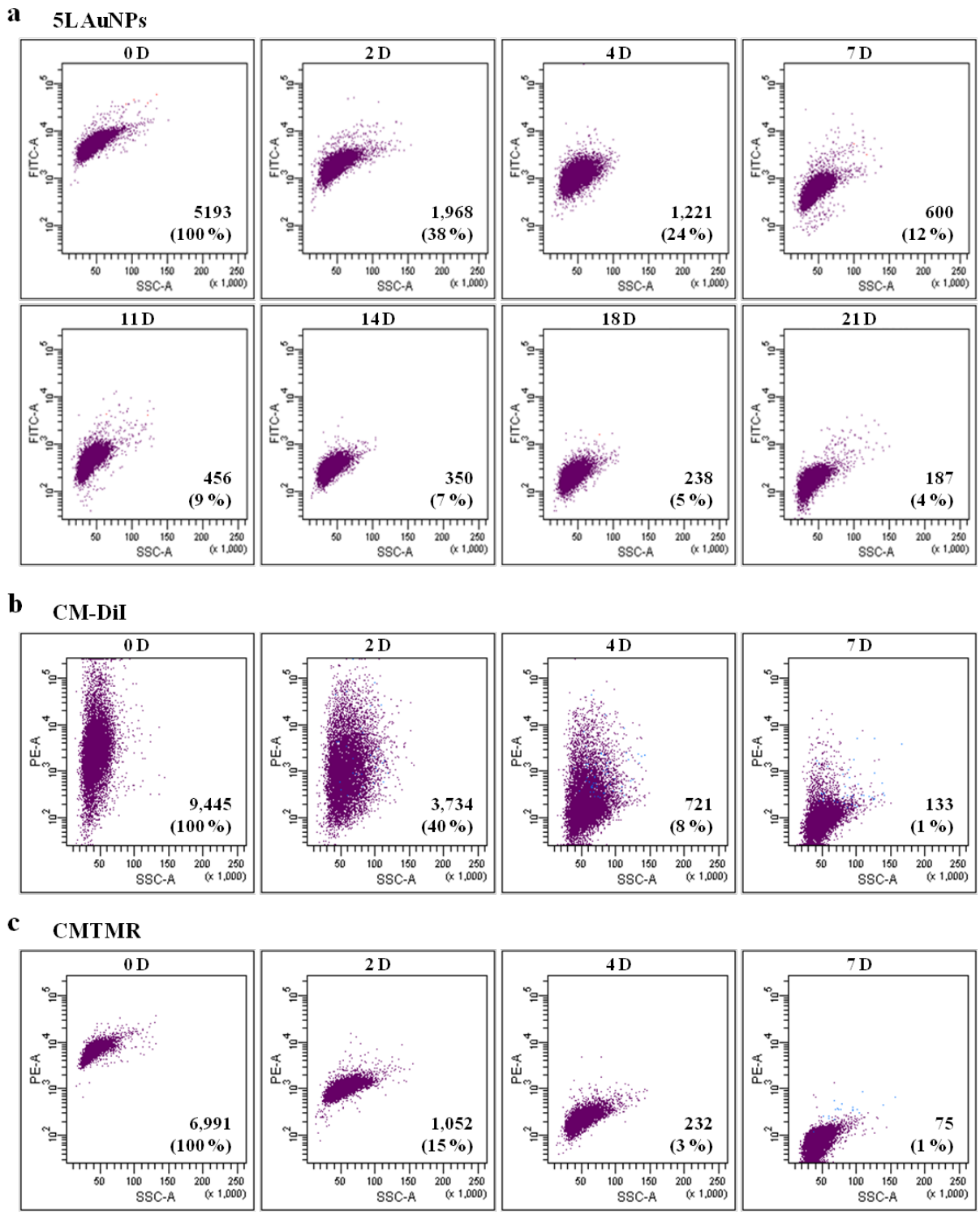

Figure S5. Cell population of Jurkat cells after treatment with 5L AuNPs. After treatment without (a) or with (b) 5L AuNPs (FITC 13.6 nmole), cell population was measured by flow cytometry for 21 days. Inserted number in each column shows the percentage of cells.

a

Control

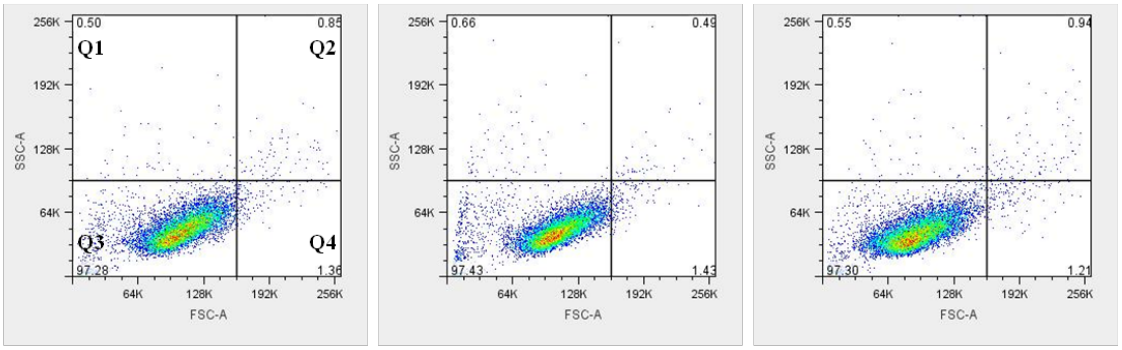

7 D 14 D 21 D

b

5L AuNPs

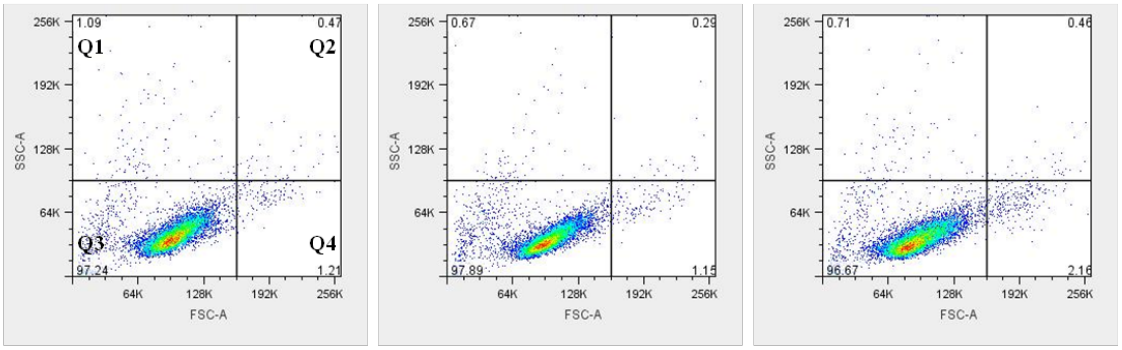

7 D 14 D 21 D

ADVANCED FUNCTIONAL MATERIALS
www.afm-journal.de

Materials Views
www.MaterialsViews.com

A Fabricated siRNA Nanoparticle for Ultralong Gene Silencing In Vivo

*Seung Koo Lee and Ching-Hsuan Tung**

Persistent gene silencing is crucially required for the successful therapeutics of short interfering RNA (siRNA). Here, a nanoparticle-based delivery system is presented which assembles by layering siRNAs between protease degradable polypeptides to extend the therapeutic window. These tightly packed nanoparticles are efficiently taken up by cells by endocytosis, and the fabricated siRNAs are gradually released following intracellular degradation of the polypeptide layers. During cell division, the particles are distributed to the daughter cells. Due to the slow degradation through the multiple layers, the particles continuously release siRNA in all cells. Using this controlled release construct, the in vivo gene silencing effect of siRNA is consistent for an ultralong period of time (>3 weeks) with only a single treatment.

1. Introduction

Short interfering RNAs (siRNAs)-mediated gene regulation in mammalian cells was first discovered about two decades ago and siRNA has since shown immense potential in treating various diseases by silencing abnormally up-regulated genes.[1–4] However, delivering the highly charged siRNA to the targeted cells and enabling the specific target gene silencing effect to persist remains challenging.[5] Although huge efforts have been invested to develop effective non-viral siRNA delivery systems, including polyplexes, micelleplexes, and exosome nanoparticles,[6,7] various physiological limitations still hinder the successful clinical translation.[8,9] The main drawbacks of gene silencing using synthetic siRNA are transient silencing due to the biodegradation of siRNA, siRNA dilution upon cell division, and its nonrenewable-nature.[10] To obtain a consistent silencing effect in vivo, it usually requires repetitive administration of the agent.[11] However, such repeated injections have resulted in a substantial impediment to patient treatment, as evidenced by decreased enrollment in clinical trials and decreased patient compliance.[12] Complete and prolonged gene silencing with a single treatment would offer enormous benefits for chronic diseases, scaling down the administration frequency in dosing schedule.[13]

To achieve long-lasting controlled release and gene silencing effects, various groups have developed novel delivery systems for slow and sustained release of the oligonucleotide or siRNA.[14–18] Several trials have also extended into primary T lymphocytes and human stem cells for prolonged gene silencing.[19,20] Although promising cell culture results were obtained in those studies, the actual in vivo efficiency remains to be demonstrated. Viral vectors have shown great efficiency in in vivo siRNA delivery,[21] however, introducing a foreign gene into patients is also a clinical concern.[22,23] Recently we have developed a fabrication method to prepare multilayer siRNA delivery nano-vector and a long-lasting nanoparticle-based fluorescent label for extended cell imaging.[24,25] Onto an inert gold nanoparticles (AuNPs), negatively charged siRNAs were layered between the oppositely charged polypeptide layers which are sensitive to proteases. The initial results with this multi-layered siRNA delivery vector suggest several advantages over other non-viral delivery systems, including uniform size, efficient cell translocation, and enhanced siRNA stability. In this study, we further optimized this nanodelivery system and determined its exceptional gene silencing effect was persistent for more than three weeks in vivo.

2. Results and Discussion

To prepare the multilayered siRNA-coated AuNPs (sRAuNPs), the negatively charged AuNPs (size: 40 nm) in water were dropped into the positively charged poly-L-lysine (PLL) solution (average M_w = 22.5 kDa; **Figure 1**a). After a 30-min incubation at room temperature with shaking and several washes with sterilized water, the positively charged PLL-coated AuNPs were added to the negatively charged siRNA solution. After incubation, free unbound siRNAs were removed by centrifugation and an additional PLL layer was added so the resulting positively charged AuNPs (sR1P) had one layer of siRNA and two layers of PLL. By repeating this procedure again, AuNPs (sR2P) with two layers of siRNA and three layers of PLL were successfully fabricated by electrostatic interactions. A zigzag pattern of the surface zeta-potential of each layer supported the success of the layering (Figure 1b). The final particle size, determined by dynamic light scattering (DLS) measurement, was found to be approximately 150 nm (Figure 1b).

Two reported siRNA sequences, termed siLuc-Na and siLuc-Ba,[1,26] against two different regions of the luciferase gene were used because maximal gene silencing effect has been reported with simultaneously applied multiple siRNAs.[27,28] sRAuNPs

Dr. S. K. Lee, Prof. Dr. C.-H. Tung
Department of Translational Imaging
The Methodist Hospital Research Institute
Weill Cornell Medical College, Houston, TX 77030, USA
E-mail: ctung@tmhs.org

DOI: 10.1002/adfm.201202777

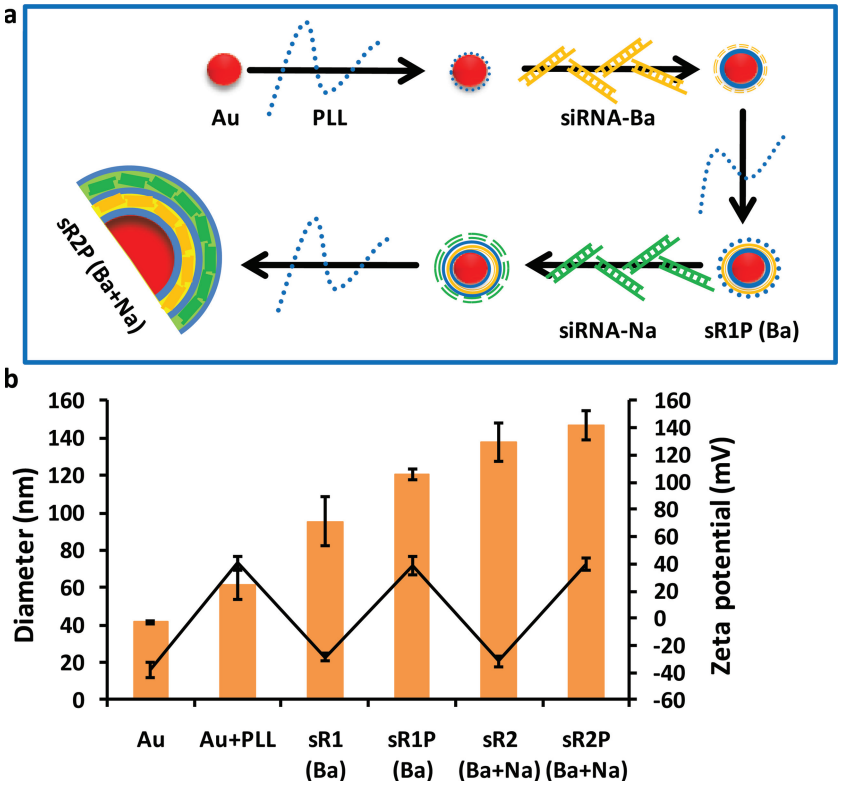

Figure 1. Preparation of the sRAuNPs. a) The process of preparing multilayered siRNA-coated AuNPs by electrostatic interaction. b) The average size (orange bar) and zeta potential (black circle) of multilayered sRAuNPs.

were fabricated with one or two siRNAs. sR2P (Ba + Na) was prepared with siLuc-Ba on the first layer and siLuc-Na on the second layer, and the order of siRNA in sR2P(Na + Ba) was reversed. A scramble siRNA (siLuc-Sc), which has the same length but randomly sequenced of siLuc-Na, was included as a negative control.

To demonstrate the success of packing and intracellular delivery of sRAuNPs, the two siRNAs, siLuc-Ba and siLuc-Na, were labeled with cy5 and cy3 fluorescent reporters, respectively. Various sRAuNPs (1.58×10^8 particles), including sR1P (Ba-cy5), sR1P (Na-cy3), and sR2P (Ba-cy5 + Na-cy3), were incubated for 24 h with MDA-MB231-luc2 cells. The presence of siRNA in cells was investigated using fluorescence microscopy (**Figure 2**). Because a cy3 or cy5 reporter was anchored to each siRNA, the fluorescence images using cy3 and/or cy5 channels reveal the location of the released siRNA. We observed a spotty fluorescence signal diffused into the cytoplasm (Figure 2b–d). The images of both cy5 and cy3 fluorescence signals after treatment with sR2P (Ba + Na) clearly indicated the presence of two kinds of siRNA (Figure 2d). These cellular-uptake data indicate that sRAuNPs enter cells without a transfection agent. Once they are internalized, the siRNA could be freed from the particles by intracellular proteolysis.

An initial gene-silencing screening experiment was performed by incubating MDA-MB231-luc2 cells with sR1P (Na), sR1P (Ba), sR2P (Na + Na), sR2P (Ba + Ba), sR2P (Na + Ba), and sR2P (Ba + Na) for 2 days (**Figure 3**a,b). A control sR2P prepared with two layers of scrambled siRNA, termed as sR2P (Sc + Sc), was also used as a negative specificity control. After incubation, the particles were washed away, and MDA-MB231-luc2 cell luminescence was measured immediately after addition of luciferin. It was determined that the luminescence was decreased to approximately 54% by sR1P (Na) (siLuc-Na 0.2 nmole; 1.58×10^8 particles) and 48% by sR1P (Ba) (siLuc-Ba 0.2 nmole; 1.58×10^8 particles) when the luminescence of untreated cells was set as 100%. With the same number of particles (1.58×10^8), the luminescence intensities of sR2P (Na + Na), sR2P (Ba + Ba), sR2P (Na + Ba), and sR2P (Ba + Na) were reduced to 46%, 44%, 38%, and 30%, respectively. As shown in Figure 3c,d, similar results were observed with LNCaP-luc2 cell lines (sR1P (Na): 50%/sR1P (Ba): 49%/sR2P (Na + Na): 46%/sR2P (Ba + Ba): 40%/sR2P (Na + Ba): 33%/sR2P (Ba + Na): 22%). When the specific siRNA was replaced with the scrambled siRNA (total siLuc-Sc 0.4 nmole), the silencing effect was insignificant. These data reveal the sequence specific silencing effect of the luciferase gene in two different cancer cell lines and show both sequences have similar inhibition effects. For comparison, commercially available and widely used Lipofectamine 2000, which is used in nucleic acid delivery, was tested in both cell lines. However, the gene silencing effect was not as remarkable as those treated with sRAuNPs even in the presence of same amount of siRNA (each siRNA 0.2 nmole; Supporting Information Figure S1). Additionally, similar luciferase signals were observed in cells treated with Lipofectamine 2000 alone and Lipofectamine 2000 formulated with siRNA. From these initial short-term inhibition results, sR2P (Ba + Na) was selected as the construct to be used in long-term gene silencing studies.

MDA-MB231-luc2 cells were treated for 2 days with sR2P (Ba + Na) in a 6-well plate (each siRNA 2.0 nmole; 1.58×10^9 particles). The cells were washed and aliquoted into separate 96-well plates for the time course study (up to 10 days). As shown in **Figure 4**a,b, the efficiency of gene silencing after treatment with sR2P (Ba + Na) on day 1 was 14% when the initial luminescent intensity of control cells was set as 100%. This significant gene silencing effect was sustained for at least 10 days (48%). In contrast, the luminescent signal increased with time as the control untreated cells divided. The luminescent signal of the untreated cells was approximately 400%, but the signal of the treated cells was less than 50% of the original signal. The experiment was forced to end at day 10, because of the physical constraint of the wells.

Although toxicity of surface modified AuNPs decorated with other polycationic polymers has been reported,[29,30] cytotoxicity of our prepared sRAuNPs was not observed. As shown in Supporting Information Figure S2, no significant toxicity was detected in any sRAuNPs-treated MDA-MB231-luc2 or

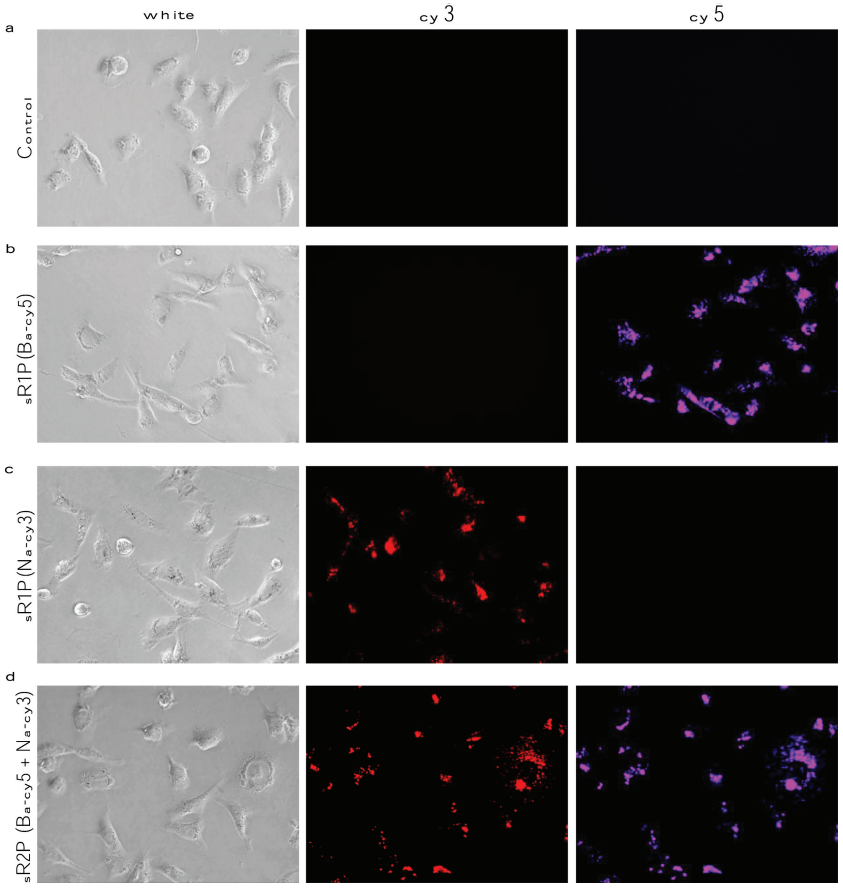

Figure 2. Cellular uptake of multilayered sRAuNPs. Images of released siRNA from various sRAuNPs were visualized using fluorescence microscopy with different filters after 24 h incubation in a) the absence or presence of b) sR1P (Ba-cy5), c) sR1P (Na-cy3), and d) sR2P (Ba-cy5 + Na-cy3) in MDA-MB231-luc2 cells.

LNCaP-luc2 cells, indicating silencing of the luciferase gene does not cause of non-specific cytotoxicity. In contrast, some toxicity was observed with Lipofectamine 2000 in both cell lines and less than 80% cells were viable.

This 10-day experiment indicated that gene silencing was effective even after cell division. With an average doubling time of 31 h for MDA-MB231 cells,[31] the sRAuNPs must effectively inhibit both the mother and daughter cells, otherwise the total luminescence should rise quickly with time. Because the unprotected siRNA is subjected to rapid nuclease degradation in cells, a persistent gene silencing effect in the daughter cells should be the result of gradually released siRNAs. Presumably, the loaded particles were re-distributed evenly to the cells during division, and the multi-layered assembly and charge-charge interaction might contribute to the prolonged gene silencing. Re-distribution of the loaded particles during cell division has recently confirmed using a similar particle which was labeled with layers of fluorescence tags.[25] The intracellular fluorescent signal was found evenly distributed to all cells and persisted for 21 days.

The in vivo gene silencing potential was evaluated further by inoculating MDA-MB231-luc2 cells (3.5×10^6) and sR2P (Ba + Na) treated MDA-MB231-luc2 cells (3.5×10^6) in both flanks nude mice. The real-time gene silencing effect was investigated non-invasively by comparing the luminescence between the inoculated tumors (**Figure 5**a). The observed gene silencing was extremely effective throughout the tested period. The relative inhibition efficiency at day 1 was 23% and was sustained until day 20 (39%). Maximal inhibition was observed at day 7 (9%). All mice tested revealed similar gene silencing efficiencies at all indicated time points (Supporting Information Figure S3), except at day 20, one mouse showed large variation (Figure 5b). As expected, there were no differences in tumor size between the untreated and sRAuNP, which targeting luciferase gene, treated tumors (Figure 5c). This data clearly show the inhibition of luciferase intensity is not caused by cytotoxic effect. These long-term inhibition results further suggest that the loaded siRNAs were able to silence its target gene in primary treated cells as well as their daughter cells for an extended period.

3. Conclusion

In summary, an ultra-long siRNA gene silencing effect was achieved both in vitro and in vivo using a functionalized nano-reservoir, which is consisted of multiple siRNA and degradable polypeptide layers. By adopting a layering deposition technology,[24,32–34] we successfully fabricated sRAuNPs by electrostatic interaction, which contain multi-layers of protease degradable PLL and synthetic siRNA. The positively charged sRAuNPs were efficiently taken up by cells and once inside the cells, the PLL was gradually degraded by intracellular proteases, resulting in the continuous release of siRNA. These intracellular sRAuNPs act as siRNA reservoirs, providing siRNA to inhibit its target genes. Upon cell division, the nano-reservoirs were distributed to daughter cells and continued to release siRNA for an extended period of time. Due to extraordinary persistent gene silencing effect, functionalized multilayered sRAuNPs are expected to have great potentials in the areas of cancer therapy, in case luciferase siRNA replaced with siRNA of onco-genes which are predominantly overexpressed in various tumors. Although this in vivo siRNA effect was performed using pretreated cells, this simple experiment demonstrated that a well-defined nanoconstruct can achieve ultra-long gene silencing effects in vivo. Currently, we are optimizing the fabrication for systemic treatment.

4. Experimental Section

Chemicals and Materials: All siRNA and poly-L-lysine (PLL) ($M_w \approx$15 000–30 000 g mol^{-1}) were obtained from Sigma-Aldrich (St. Louis, MO). Bare AuNPs (40 nm) particles were purchased from BB

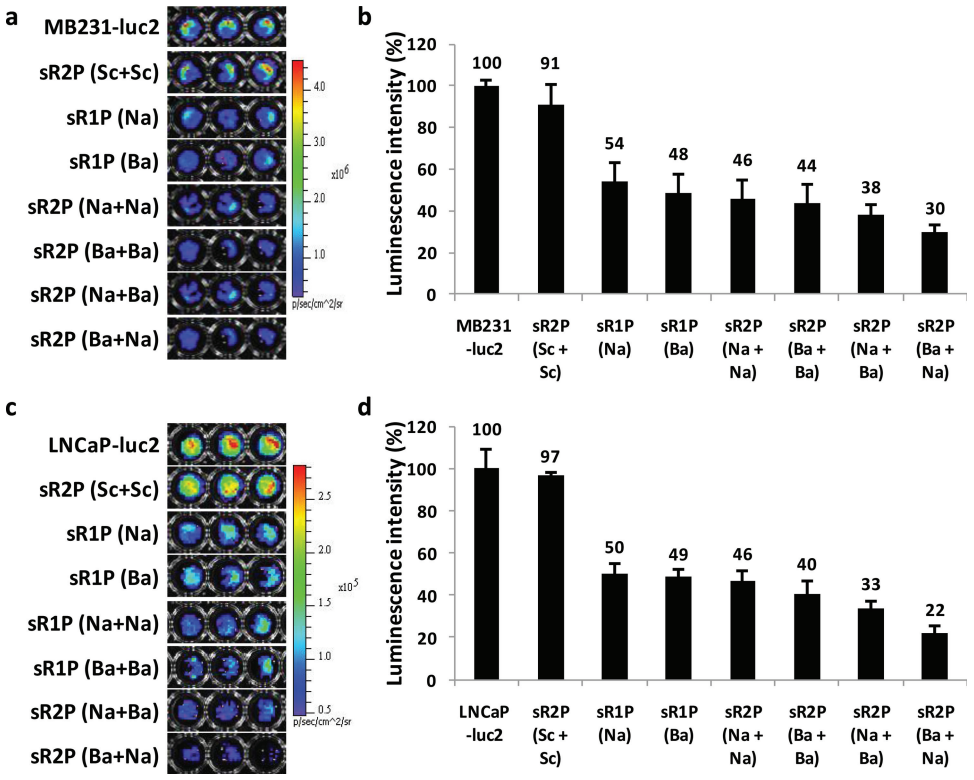

Figure 3. In vitro gene-silencing effect of multilayered sRAuNPs. The luminescence signal and the luminescence intensity (photons s^{-1}) in a,b) MDA-MB231-luc2 cells or c,d) LNCap-luc2 after incubation for 2 days with various sRAuNPs. The luminescence intensity of each cell line without treatment was set as 100%. The results are representative of three independent experiments.

International (Cardiff, UK), Lipofectamine 2000 was from Invitrogen (Carlsbad, CA), D-Luciferin was from Regis Technologies (Morton Grove, IL), Matrigel (phenol red-free) was from BD Biosciences (San Jose, CA) and CellTiter aqueous one solution was from Promega (Madison, WI).

Preparation and Characterization of Multilayered sRAuNPs: Using layer by layer (LbL) fabrication method, multilayers of siRNA and PLL were successfully deposited on Au surface. The sequences of siLuc-Ba[26] against luciferase are sense strand:

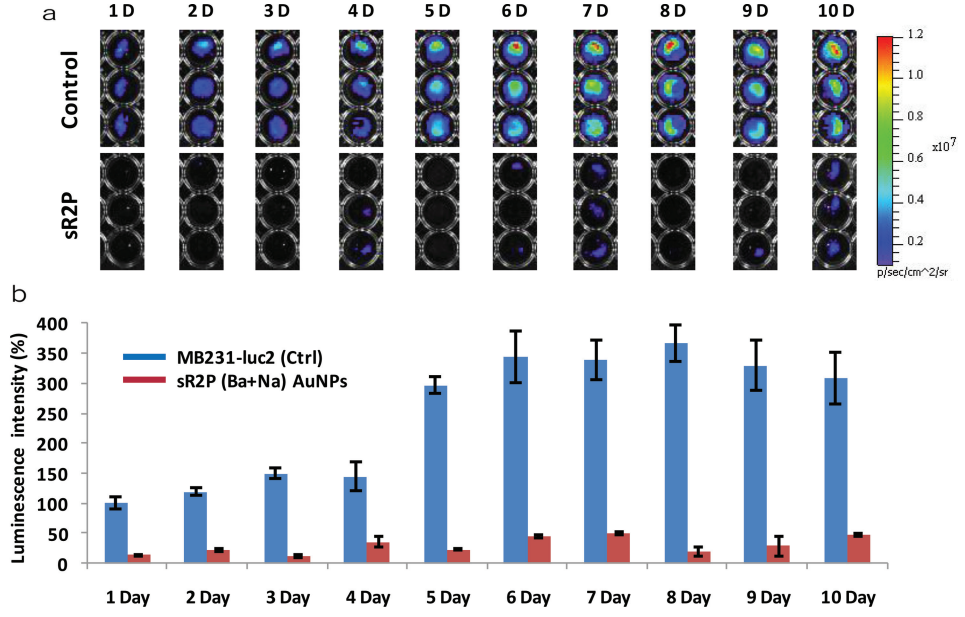

Figure 4. Prolonged gene-silencing effect of multilayered sRAuNPs. a,b) The prolonged gene silencing effect was also evaluated by measuring the luminescence signal for up to 10 days after treatment with sR2P (Ba + Na) in MDA-MB231-luc2 cells. The luminescence intensity without treatment at day 1 was set as 100%. The results are representative of three independent experiments.

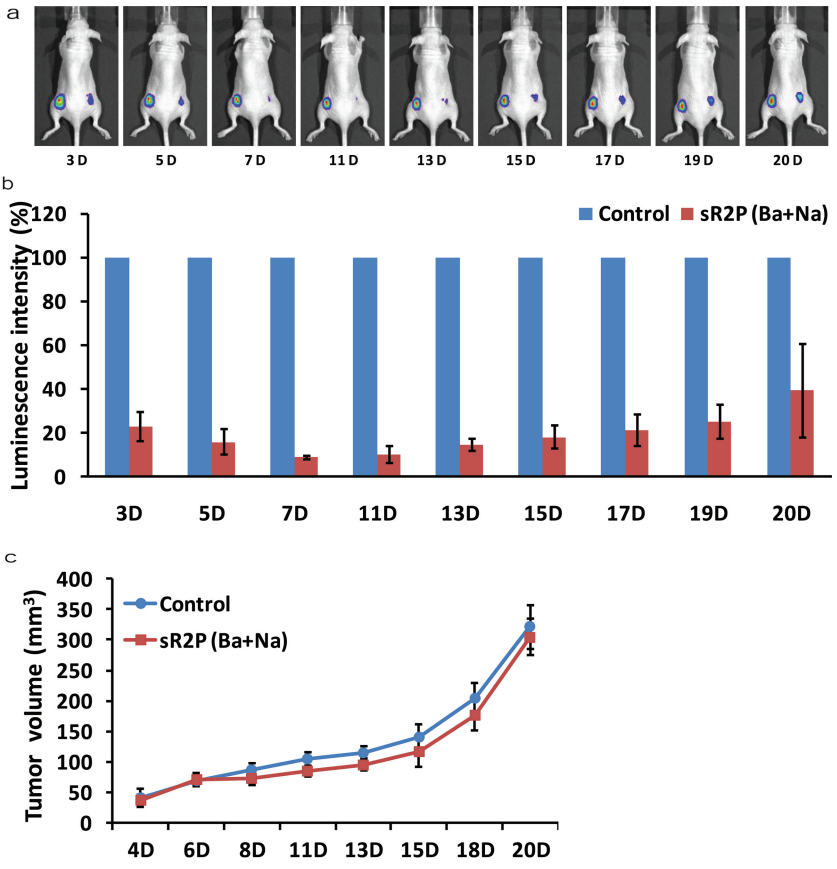

Figure 5. In vivo gene-silencing effect of multilayered sRAuNPs. a) The luminescence signal and b) the luminescence intensity of non-treated (left flank) or sR2P (Ba + Na) treated MDA-MB231-luc2 cells (right flank) were collected up to 20 days after implantation by IVIS-200. The luminescence intensity (photons s^{-1}) of non-treated cells (left flank) at each time point was set as 100%. c) Comparison of the tumor size of control versus the sR2P (Ba + Na) treated group during 20 days. Data represent the tumor volume (mean ± SEM) for each group.

5′-UUAAUCAGAGACUUCAGGCGGUdTdT-3′, antisense strand: 5′-ACCGCCUGAAGUCUCUGAUUAAdTdT-3′, siLuc-Na[1] are sense strand: 5′-CGUACGCGGAAUACUUCGAdTdT-3′, antisense strand: 5′ UCGAAGUAUUCCGCGUACGdTdT-3′, and of control nonsnese siRNA (siLuc-ctrl) are sense strand: 5′-AGCUUCAUAAGGCGCAUGCdTdT-3′ and antisense strand: 5′-GCAUGCGCCUUAUGAAGCU-3dTdT-3′). AuNPs solution (3.15×10^9 particles in 0.7 mL) was added dropwisely onto a PLL solution (0.5 mL of 5 mg mL^{-1}) in pure water. After incubating for 30 min in the dark with gentle shaking, the solution was centrifuged for 30 min at 16,100 g using a micro centrifuge (Eppendorf, Hauppauge, NY). The supernatant was removed, and the gel-like deep red pellet was re-suspended with pure water and centrifuged for 30 min at 16,100 g. PLL coated AuNPs were stored in pure water after additional wash. Next polyelectrolyte layer was deposited by adding PLL coated AuNPs (in 0.5 mL pure water) to siRNA solution (4.0 nmole, 0.5 mL). The reaction solution was incubated in the dark for 30 min with gentle shaking, followed by three washes. The deposition procedures were repeated to have total 5 layers of polyelectrolytes (3 layers of PLL and 2 layers of siRNA). Sizes and zeta potentials of AuNPs in water were measured by Zetasizer Nano-ZS (Malvern, Worcestershire, UK) according to the manufacturer's instruction.

Cell Lines: The human breast cancer cell line stably expressing firefly luciferase (MDA-MB231-luc2) and the human prostate cancer cell line stably expressing firefly luciferase (LNCaP-luc2) were purchased from Caliper (Alameda, CA). MDA-MB231-luc2 cell line were cultured in DMEM medium (Mediatech Inc., Manassas, VA), while LNCaP-luc2 cell line were cultured in RPMI 1640 medium (Thermo Scientific, Rockford, IL) and both cell lines were supplemented with 2 mM L-glutamine, 100 U mL^{-1} penicillin, 100 mg mL^{-1} streptomycin, and 10% heat-inactivated fetal bovine serum (Sigma-Aldrich) in a humidified atmosphere of 5% CO_2 at 37 °C.

Live Cell Imaging for Cellular Uptake of sRAuNPs: A cy5 fluorochrome was tagged on the 5′ end of the sense siLuc-Ba and a cy3 fluorochrome was tagged on the 5′ end of the sense siLuc-Na. Fluorescence images of live cells were acquired using a fluorescence microscopy system (Olympus, Tokyo, Japan). Briefly, MDA-MB231-luc2 cells were seeded on a 96-well black clear-bottom culture plate (Corning Life Sciences, Pittston, PA) at a density of 5.0×10^3 cells per well. After 1 day, the culture medium was replaced with sR1P (Ba-cy5), sR1P (Na-cy3) or sR2P (Ba-cy5 + Na-cy3) AuNPs (1.58×10^8 particles) containing medium, and further cultured for 24 h. Cells were then washed twice with phosphate buffered saline (PBS) and cultured in the phenol red-free medium and imaged with a fluorescence microscopy.

Cytotoxicity Assessment of sRAuNPs: A cell proliferation assay was performed to assess the cytotoxicity of Lipofectamine 2000 (Invitrogen) and the preparations of sRAuNPs. Briefly, MDA-MB231-luc2 cells were collected by trypsinization, counted, and plated in a 96-well culture plate at a density of 5×10^3 (or 2.5×10^4 of LNCaP-luc2) cells per well. One day later, sRAuNPs (1.58×10^8 particles) or Lipofectamine 20000 (0.2 µL) were added and the cells were further cultured for 48 h. For Lipofectamine 20000, due to toxicity issue, fresh complete medium were replaced after incubation with Lipofectamine 2000 for 4 h and further cultured for additional 44 h. At day 3, 20 µL CellTiter solution (Promega) was added to each well after replacing with fresh medium and incubated for an additional 3 h, and then the absorbance of the solution was measured at 490 nm using a Spectramax M2 plate reader (Molecular Devices).

In Vitro Gene Silencing Effect: For the examination of the gene silencing effect in vitro, bioluminescence measurement was performed after incubating with various multilayered AuNPs. Briefly, MDA-MB-231 cells were seeded in a 96-well black clear bottom culture plate at a density of 5×10^3 (or 2.5×10^4 of LNCaP-luc2) cells per well. One day later, different sRAuNP (1.58×10^8 particles) were added to each well and cultured for additional 48 h and replaced with fresh medium. Manufacturer's instruction was followed for transfection with Lipofectamine 2000. Bioluminescence measurement was performed using IVIS-200 (Caliper) immediately after addition 125 µg mL^{-1} of D-Luciferin (Regis). To investigate in vitro long-term gene silencing effects, MDA-MB231-luc2 cells were seeded in a 6-well culture plate (BD Falcon, San Jose, CA) at a density of 2.0×10^5 cells per well. One day later, sR2P (Ba + Na) (1.58×10^9 particles) were added to each well and cultured for additional 48 h. sRAuNPs treated MDA-MB231-luc2 cells in 6-well plate were collected by trypsinization, counted, and re-plated in a 96-well black clear bottom culture plate at a density of 1.5×10^3 cells per well. Bioluminescence measurement of each well appropriate from day 1 to day 10 was performed using IVIS-200 (Caliper) immediately after addition 125 µg mL^{-1} of D-Luciferin (Regis).

In Vivo Gene Silencing Effect: All animal studies were performed in compliance with the approved animal protocols and guidelines of Institutional Animal Care and Use Committee at The Methodist Hospital Research Institute. To evaluate gene silencing effect in vivo,

bioluminescence measurement was performed after implantation of sR2P (Ba + Na) treated or non-treated MDA-MB231-luc2 cells to female nude (nu/nu) mice. MDA-MB-231 cells were seeded in a 6-well culture plate (BD Falcon) at a density of 2.0×10^5 cells per well. One day later, sR2P (Ba + Na) (1.58×10^9 particles) were added to each well and cultured for additional 48 h. sRAuNPs treated or non-treated MDA-MB231-luc2 cells were collected by trypsinization, counted, and implanted bilaterally (3.5×10^6 cells in 200 μL of PBS including 50 μL of Matrigel) in the posterior flanks of mice. Bioluminescence imaging was carried out with a group of 3 mice. Bioluminescence of tumor-bearing mice was imaged using a small animal optical imaging system (IVIS-200, Caliper) immediately after injecting 2 mg (in 150 μL of PBS) of D-Luciferin (Regis) per mouse up to 20 days after cell implantation. Tumors were measured at the indicated time with digital calipers, and volumes were calculated according to the formula[35] as $0.5 \times (\text{length}) \times (\text{width})^2$.

Supporting Information

Supporting Information is available from the Wiley Online Library or from the author.

Acknowledgements

The authors thank Ms. Myung Shin Han for her technical support in animal imaging. This study was supported in part by NIH CA135312, DOD W81XWH-11-1-0442, and the Golfers Against Cancer Foundation.

Received: September 24, 2012
Revised: November 26, 2012
Published online: February 18, 2013

[1] S. M. Elbashir, J. Harborth, W. Lendeckel, A. Yalcin, K. Weber, T. Tuschl, *Nature* **2001**, *411*, 494.
[2] P. D. Zamore, *Cell* **2006**, *127*, 1083.
[3] D. Bumcrot, M. Manoharan, V. Koteliansky, D. W. Sah, *Nat. Chem. Biol.* **2006**, *2*, 711.
[4] J. C. Burnett, J. J. Rossi, *Chem. Biol.* **2012**, *19*, 60.
[5] T. Lobovkina, G. B. Jacobson, E. Gonzalez-Gonzalez, R. P. Hickerson, D. Leake, R. L. Kaspar, C. H. Contag, R. N. Zare, *ACS Nano* **2011**, *5*, 9977.
[6] D. J. Gary, H. Lee, R. Sharma, J. S. Lee, Y. Kim, Z. Y. Cui, D. Jia, V. D. Bowman, P. R. Chipman, L. Wan, Y. Zou, G. Mao, K. Park, B. S. Herbert, S. F. Konieczny, Y. Y. Won, *ACS Nano* **2011**, *5*, 3493.
[7] L. Alvarez-Erviti, Y. Seow, H. Yin, C. Betts, S. Lakhal, M. J. Wood, *Nat. Biotechnol.* **2011**, *29*, 341.
[8] C. Schmidt, *Nat. Biotechnol.* **2011**, *29*, 93.
[9] C. V. Pecot, G. A. Calin, R. L. Coleman, G. Lopez-Berestein, A. K. Sood, *Nat. Rev. Cancer* **2011**, *11*, 59.
[10] Y. Takabatake, Y. Isaka, M. Mizui, H. Kawachi, S. Takahara, E. Imai, *Biochem. Biophys. Res. Commun.* **2007**, *363*, 432.
[11] W. M. Merritt, Y. G. Lin, W. A. Spannuth, M. S. Fletcher, A. A. Kamat, L. Y. Han, C. N. Landen, N. Jennings, K. De Geest, R. R. Langley, G. Villares, A. Sanguino, S. K. Lutgendorf, G. Lopez-Berestein, M. M. Bar-Eli, A. K. Sood, *J. Natl. Cancer Inst.* **2008**, *100*, 359.
[12] T. Tanaka, L. S. Mangala, P. E. Vivas-Mejia, R. Nieves-Alicea, A. P. Mann, E. Mora, H. D. Han, M. M. Shahzad, X. Liu, R. Bhavane, J. Gu, J. R. Fakhoury, C. Chiappini, C. Lu, K. Matsuo, B. Godin, R. L. Stone, A. M. Nick, G. Lopez-Berestein, A. K. Sood, M. Ferrari, *Cancer Res.* **2010**, *70*, 3687.
[13] K. Raemdonck, R. E. Vandenbroucke, J. Demeester, N. N. Sanders, S. C. De Smedt, *Drug Discovery Today* **2008**, *13*, 917.
[14] S. Bulut, T. S. Erkal, S. Toksoz, A. B. Tekinay, T. Tekinay, M. O. Guler, *Biomacromolecules* **2011**, *12*, 3007.
[15] R. E. Vandenbroucke, B. G. De Geest, S. Bonne, M. Vinken, T. Van Haecke, H. Heimberg, E. Wagner, V. Rogiers, S. C. De Smedt, J. Demeester, N. N. Sanders, *J. Gene Med.* **2008**, *10*, 783.
[16] S. Mehrotra, I. Lee, C. Chan, *Acta Biomater.* **2009**, *5*, 1474.
[17] H. Fujimoto, K. Kato, H. Iwata, *Anal. Bioanal. Chem.* **2010**, *397*, 571.
[18] X. Zhang, A. Kovtun, C. Mendoza-Palomares, M. Oulad-Abdelghani, F. Fioretti, S. Rinckenbach, D. Mainard, M. Epple, N. Benkirane-Jessel, *Biomaterials* **2010**, *31*, 6013.
[19] A. Mantei, S. Rutz, M. Janke, D. Kirchhoff, U. Jung, V. Patzel, U. Vogel, T. Rudel, I. Andreou, M. Weber, A. Scheffold, *Eur. J. Immunol.* **2008**, *38*, 2616.
[20] M. Rosner, N. Siegel, C. Fuchs, N. Slabina, H. Dolznig, M. Hengstschlager, *Nat. Protoc.* **2010**, *5*, 1081.
[21] L. Suckau, H. Fechner, E. Chemaly, S. Krohn, L. Hadri, J. Kockskamper, D. Westermann, E. Bisping, H. Ly, X. Wang, Y. Kawase, J. Chen, L. Liang, I. Sipo, R. Vetter, S. Weger, J. Kurreck, V. Erdmann, C. Tschope, B. Pieske, D. Lebeche, H. P. Schultheiss, R. J. Hajjar, W. C. Poller, *Circulation* **2009**, *119*, 1241.
[22] S. Hacein-Bey-Abina, C. Von Kalle, M. Schmidt, M. P. McCormack, N. Wulffraat, P. Leboulch, A. Lim, C. S. Osborne, R. Pawliuk, E. Morillon, R. Sorensen, A. Forster, P. Fraser, J. I. Cohen, G. de Saint Basile, I. Alexander, U. Wintergerst, T. Frebourg, A. Aurias, D. Stoppa-Lyonnet, S. Romana, I. Radford-Weiss, F. Gross, F. Valensi, E. Delabesse, E. Macintyre, F. Sigaux, J. Soulier, L. E. Leiva, M. Wissler, C. Prinz, T. H. Rabbitts, F. Le Deist, A. Fischer, M. Cavazzana-Calvo, *Science* **2003**, *302*, 415.
[23] X. Guo, L. Huang, *Acc. Chem. Res.* **2012**, *45*, 971.
[24] S. K. Lee, M. S. Han, S. Asokan, C. H. Tung, *Small* **2011**, *7*, 364.
[25] S. K. Lee, M. S. Han, C. H. Tung, *Small* **2012**, *8*, 3315.
[26] K. Chang, S. J. Elledge, G. J. Hannon, *Nat. Methods* **2006**, *3*, 707.
[27] S. Wang, Z. Shi, W. Liu, J. Jules, X. Feng, *BMC Biotechnol.* **2006**, *6*, 50.
[28] M. E. Peter, *Oncogene* **2010**, *29*, 2161.
[29] D. A. Giljohann, D. S. Seferos, W. L. Daniel, M. D. Massich, P. C. Patel, C. A. Mirkin, *Angew. Chem. Int. Ed.* **2010**, *49*, 3280.
[30] M. L. Read, S. Singh, Z. Ahmed, M. Stevenson, S. S. Briggs, D. Oupicky, L. B. Barrett, R. Spice, M. Kendall, M. Berry, J. A. Preece, A. Logan, L. W. Seymour, *Nucleic Acids Res.* **2005**, *33*, e86.
[31] N. Watanabe, E. Okochi, M. Mochizuki, T. Sugimura, T. Ushijima, *Cancer Res.* **2001**, *61*, 7739.
[32] C. M. Jewell, D. M. Lynn, *Adv. Drug Delivery Rev.* **2008**, *60*, 979.
[33] N. Reum, C. Fink-Straube, T. Klein, R. W. Hartmann, C. M. Lehr, M. Schneider, *Langmuir* **2010**, *26*, 16901.
[34] T. Suma, K. Miyata, Y. Anraku, S. Watanabe, R. J. Christie, H. Takemoto, M. Shioyama, N. Gouda, T. Ishii, N. Nishiyama, K. Kataoka, *ACS Nano* **2012**, *6*, 6693.
[35] K. Kim, G. Chadalapaka, S. S. Pathi, U. H. Jin, J. S. Lee, Y. Y. Park, S G. Cho, S. Chintharlapalli, S. Safe, *Mol. Cancer Ther.* **2012**, *11*, 1852.